1.2-MICRON MULTI-SECTION QUANTUM DOT SUPERLUMINESCENT DIODES

BY

THERESE A. SAIZ

B.S., UNIVERSITY OF NEW MEXICO, 2005

THESIS

Submitted in Partial Fulfillment of the
Requirements for the Degree of

Master of Science
Electrical Engineering

The University of New Mexico
Albuquerque, New Mexico

August, 2008

DEDICATION

To Francesca Carrillo

ACKNOWLEDGMENTS

The research in this thesis was performed at the Center for High Technology Materials (CHTM), at the University of New Mexico. First I would like to thank my advisor Luke F. Lester for his expert guidance and direction, and for giving me the opportunity to pursue a thesis master's degree.

I thank our post-doctoral student Yongchun Xin for his guidance in the lab and all his never-ending patience and help with this thesis work.

I thank Anthony Martinez for his step by step guidance in the clean-room and for an excellent introduction to SLD theory and testing procedures. Thanks for making my introduction to graduate school a pleasant one.

I thank Professor Sanjay Krishna for reviewing my thesis and providing valuable comments and suggestions.

I thank Professor Frederic Grillot for his help and insightful comments on completing this thesis.

I also thank my group members Mohamed El-Emawy, and Furqan Chiragh for their support in the SLD project. Mohamed processed the SLD material for this project. I thank Nader Naderi, Tron Nilsen, Chang-Yi Lin, Mike Pochet, and Yan Li for their help during my graduate studies.

And finally I thank my parents for all their love and support. Thanks mom and dad!

1.2-MICRON MULTI-SECTION QUANTUM DOT SUPERLUMINESCENT DIODES

BY

THERESE A. SAIZ

ABSTRACT OF THESIS

Submitted in Partial Fulfillment of the
Requirements for the Degree of

Master of Science
Electrical Engineering

The University of New Mexico
Albuquerque, New Mexico

August, 2008

1.2-MICRON MULTI-SECTION QUANTUM DOT SUPERLUMINSECENT DIODES

by

Therese A. Saiz

B.S., Electrical Engineering, University of New Mexico, 2005
M.S., Electrical Engineering, University of New Mexico, 2008

ABSTRACT

Superluminescent diodes (SLD) with a center wavelength of 1.2μm are of interest for use in medical imaging of skin tissue especially in the field of optical coherence tomography (OCT). In this thesis a ridge-waveguide multi-section quantum dot SLD that emits at 1.2μm with a bandwidth greater than 100nm and a power greater than 0.2mW is presented. The multi-section SLD allows simultaneous tuning of the ground state emission and excited state emission, resulting in wide bandwidth and high power. Theoretical equations describing the intensity output of the multi-section SLD configuration are presented. It is found that these equations are able to closely predict the measured SLD intensity as function of wavelength given measured gain and spontaneous emission spectra of the quantum dot active region. The gain and spontaneous emission data are derived from the improved segmented contact measurement technique that is especially compatible with the multi-section device approach and the stringent requirements on accuracy imposed by the low-gain quantum dot materials. Within the

theoretical model, various approaches to simulating the SLD spectra are also investigated and compared.

TABLE OF CONTENTS

LIST OF FIGURES

LIST OF TABLES

Chapter 1 - Introduction

1.1 SLD Overview

A superluminescent diode (SLD) is an edge-emitting optoelectronic device that is a hybrid of an LED and a semiconductor optical amplifier (SOA). The overall purpose of the SLD is to provide a high power, broadband incoherent source with a Gaussian spectral output through the use of amplified spontaneous emission [1]. A secondary goal of the device is that the emitted light be easily coupled into a single-mode fiber. The SLD has a broader bandwidth, usually expressed in terms of the full width at half maximum (FWHM) of the emitted power as a function of wavelength, than a laser diode (LD) and higher power than a typical light emitting diode (LED) as shown in Figure 1-1.

However, like any hybrid device, there are some tradeoffs in the SLD that can best be described by comparing it to the LD and LED. The light emission in an LD is dominated by stimulated emission that is coherent and extremely narrow band. In comparison, the light exiting an LED is all spontaneous emission, incoherent, and very broadband [2]. Since a SLD is made from a single-pass amplifier of spontaneous emission, the light exiting the emitting facet of a SLD is mostly incoherent, but there is some coherence due to the stimulated emission process used in the amplification that undesirably narrows the emission spectrum [3]. Also due to the residual reflection from the facets in a SLD, there is an associated Fabry-Perot gain ripple in the emission spectrum. Thus, although higher power can be realized by electrically pumping the SLD

at higher currents or by lengthening the cavity, the tradeoff is that the emission spectrum narrows and obtains a spectrally-modulated emission. A depiction of the electroluminescence curves can be seen in Figure 1-1.

The light-versus-current (L-I) curves for the SLD, LD, and LED are shown in Figure 1-2 [3]. The power of an LED varies linearly with the current unlike a laser, which has a sharp turn when it reaches threshold. A SLD L-I curve is more similar to that of a laser, except threshold is not as pronounced.

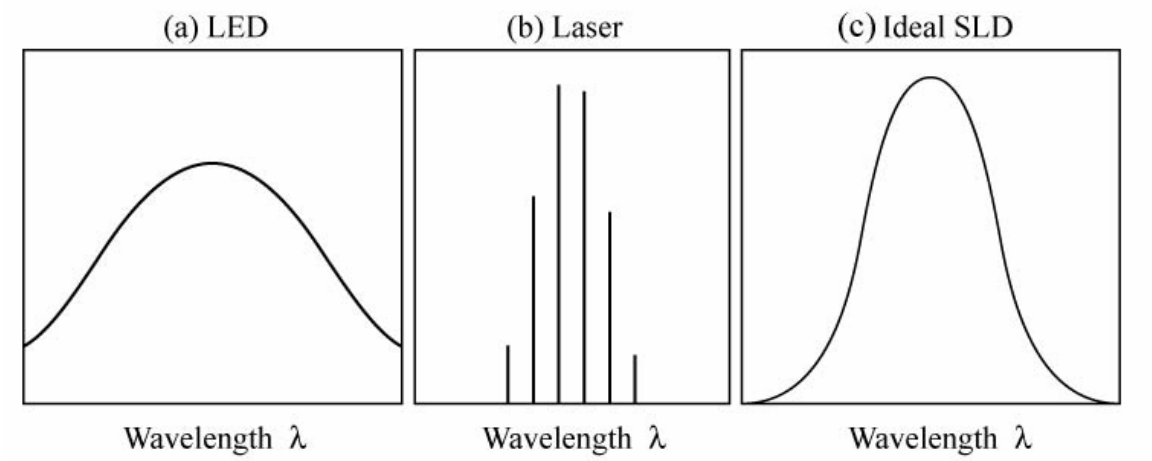

Figure 1-1. Generic schematic of electroluminescence curve for (a) LED (b) multimode laser (c) ideal SLD[3]

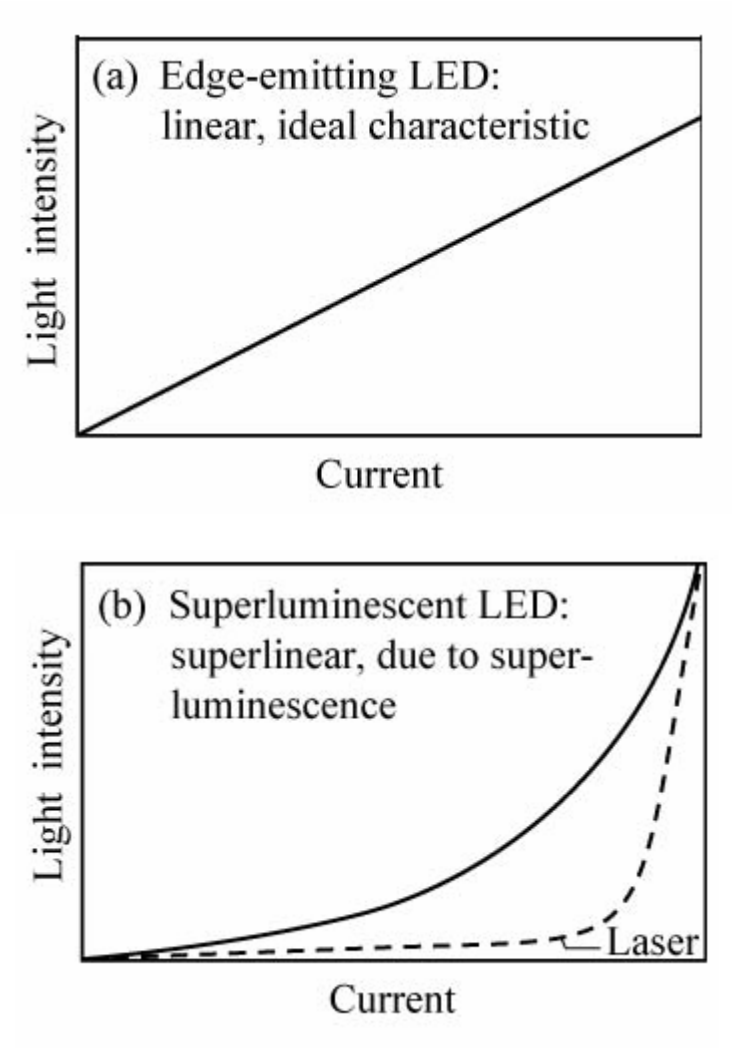

Figure 1-2. Generic schematic of L-I curves for an (a) LED, (b) laser diode, and SLD [3]

1.2 SLD Applications

SLDs have a variety of uses in applications that require a light source with a broad emission spectrum. Their most popular uses are in the fields of Optical Coherence Tomography (OCT), gyroscopes, and fiber-optic sensors [4]. OCT is a type of medical imaging which uses a broad-band light source such as a SLD [5]. It produces high-resolution two-dimensional cross-sectional images of living tissue. It is based on low-coherence interferometry. Femtosecond lasers and external cavity scanning lasers are common light sources used in OCT. However, they are expensive and difficult to operate [6]. The broad bandwidth and low cost of SLDs make them promising sources for OCT [7]. Using compact broad-band optical sources, like SLDs, and fiber optics, OCT systems can be portable. A few factors important to the OCT optical source include longitudinal resolution, penetration into the tissue, high irradiance, and overall system cost. A wider bandwidth will produce better resolution. A graph relating the longitudinal resolution to the optical source bandwidth is shown in Figure 1-3 [8].

OCT with resolutions of 10μm-15μm has been used in applications such as cardiology, gastroenterology, and ophthalmology [8]. However, skin cells are on the order of 20μm, so a resolution of about 5μm is required for diagnosing an aberrant cell. As can be seen from Figure 1-3, a bandwidth of 150nm will produce a resolution of 5μm, therefore a bandwidth of at least 150nm is ultimately desirable for high resolution OCT [8].

The furthest penetration into the skin has been achieved with sources emitting at wavelengths between 1200 and 1800nm[7]. An emission peak of 1200nm is optimum to reduce scattering in the tissue. Higher energy light such as blue and UV have a short penetration depth and can only give images less than a few hundred microns thick. Wavelengths above 2500 nm are also not ideal because of the vibrational absorption of water [7].

OCT requires a high-powered source to fill the need for wide dynamic range and high detection sensitivity for imaging backscattering structures deep inside tissue. SLDs used for OCT at 1300nm require a general output power between 1mW and 5mW. [7]

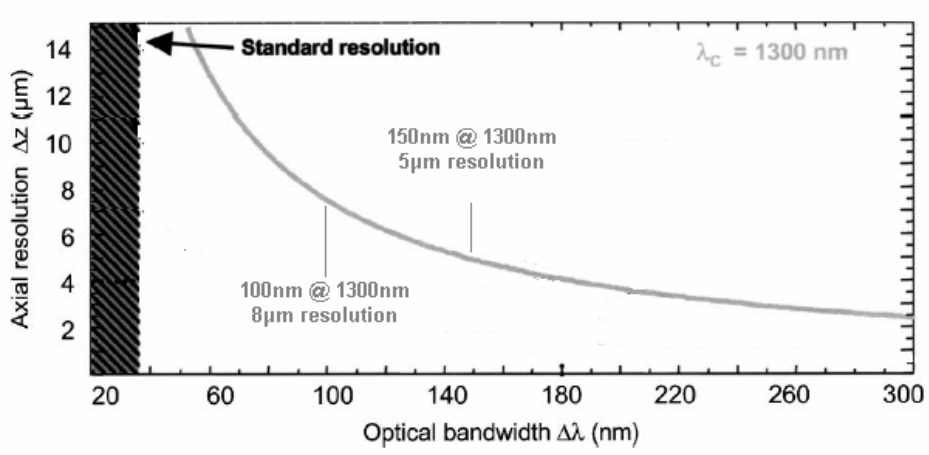

Figure 1-3. Longitudinal resolution versus optical source bandwidth. Standard OCT resolution is worse than 14μm. A bandwidth of 100nm yields a resolution of 8μm while a bandwidth of 150nm yields a resolution of 5μm.[8]

1.3 Quantum Dots

Currently nanoscience and nanotechnology are important areas of research because of their ability to provide advances in modern physics, chemistry, biology, and many areas of engineering technology [9, 10]. Semiconductor nanostructures such as quantum dots (QDs) are one of the many interesting topics in the field of nanotechnology. Semiconductor quantum dots exhibit properties that are superior to bulk material and quantum wells. They are considered to be zero-dimensional (0D) systems, which means they enable three dimensional confinement of electron-hole pairs. This characteristic results in discrete, quantized energy levels and a delta function like density of states, and gives the dots advantages over bulk, quantum well, and quantum wire structures.

The bulk density-of-states is continuous as shown below in Figure 1-4, and is considered a 3D system, which means that it has no confinement in any direction. Quantum wells have one dimension of confinement and the density of states decreases and looks like a step function. The quantum wire, a 1-dimensional system, has two-dimensional confinement, further decreasing the density of states. The quantum dot is a zero-dimensional system that exhibits 3D confinement, reducing the density of states to delta functions. This delta-function density of states gives the quantum dot advantages over other structures in semiconductor lasers (a close cousin of the SLD), such as a low threshold current density, high T_0 value, a relatively temperature-insensitive threshold current, improved high-speed modulation, decreased linewidth enhancement factor, and broader bandwidth from an easily saturated gain and absorption.

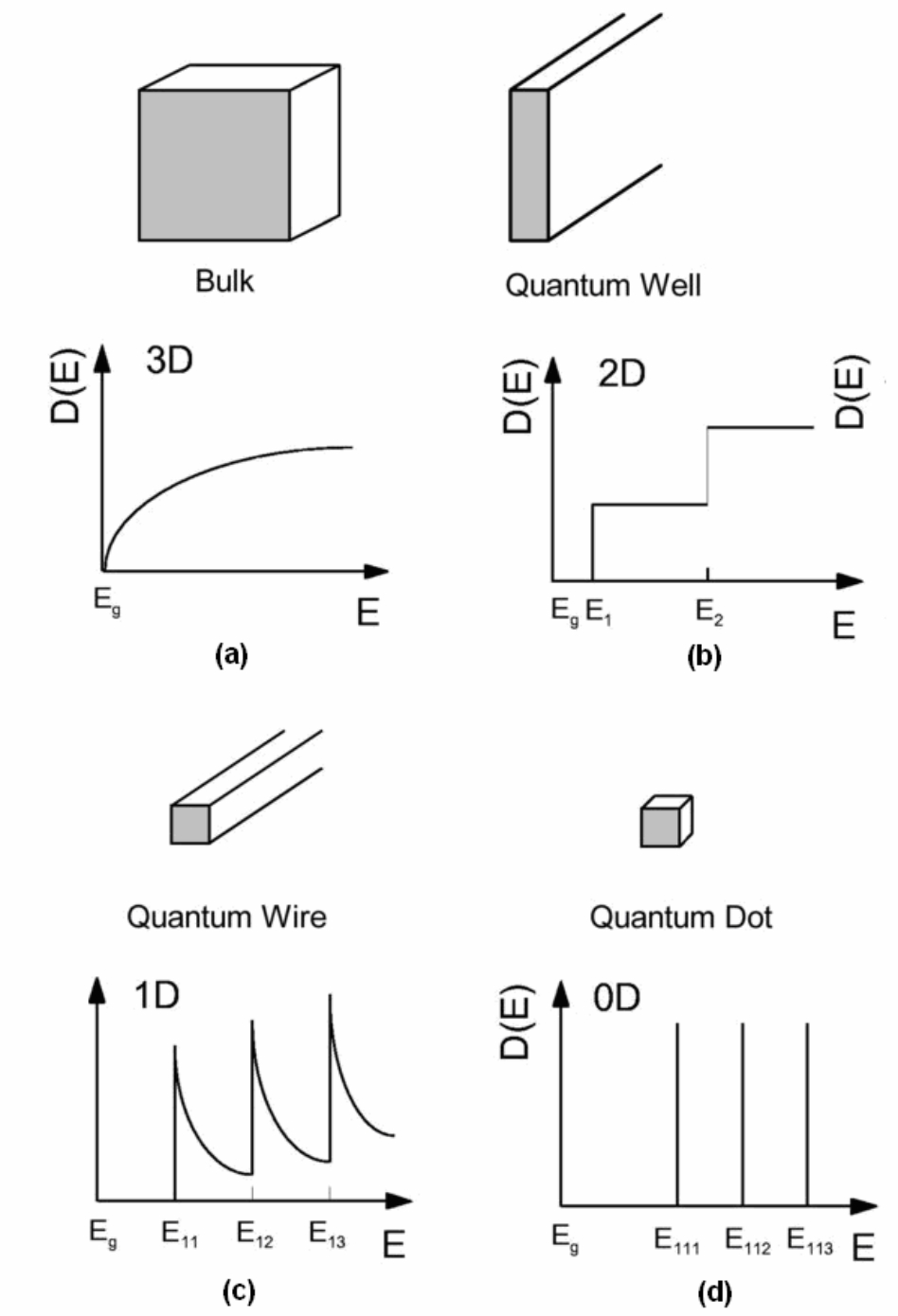

Figure 1-4. Density of states for (left) bulk, (left center) quantum well, (right center) and (right) quantum dot. The quantum dot have [15]

A real, epitaxial quantum dot is a nanoscale semiconductor structure in the shape of a disk or square pyramid that is embedded in a wider bandgap semiconductor. The dot confining dimensions are near that of the De Broglie wavelength of the electron. Quantum dots are used in a variety of technical applications including but not limited to lasers, infrared detectors, optical amplifiers, charge storage devices, and quantum information processing devices [11]. Today quantum dots can be made into defect-free islands that are self-organized and self-assembled. These defect-free islands are realized by self-organized epitaxial growth of mismatched semiconductor heterostructures. Most of the research of epitaxial semiconductor quantum dots has been done with GaAs and InP- based materials but progress is being made with other materials such as group III-nitrides and silicon [12]. Quantum dots are generally grown in layers, with each layer separated by a barrier material. Each layer of dots can contain 10^{10} - 10^{12} of dots per square centimeter. The dots can vary slightly in shape and size with a Gaussian distribution, contributing to a broader emission bandwidth due to the variation in the bandgap from the quantum size effect. The peak wavelength of InAs quantum dots grown on GaAs can be tuned over the range of 950 to 1330 nm. The tuning is achieved by varying the size, shape and composition of the dot, which is done by varying growth parameters. There is a special type of dot structure called chirped quantum dots, in which each quantum dot layer in the active region can be tuned to a slightly different peak emission wavelength [13]. In one special case, optimal chirping of the QD active region results when each layer, or every other layer, has a peak wavelength corresponding to the

half power wavelength of an adjacent layer. This results in an even broader and flatter bandwidth.[4]

The wider bandwidth is especially useful for SLDs. The quantum dot discrete energy levels cause the SLD output spectrum to have several distinct humps, depending on the current pump level. If pumped at low current levels, where the ground state energy level has not yet filled, the output spectrum will have one hump. If pumped at a higher current level the ground state will fill and emission from the first excited state will emerge. When pumped even higher the first excited state emission will dominate the emission spectrum. The result is an oddly shaped output emission spectrum with two humps at different intensity levels, the excited state emission being higher. The best bandwidth scenario occurs when the excited state emission and the ground state emission are at the same intensity as seen in Figure 1-5.

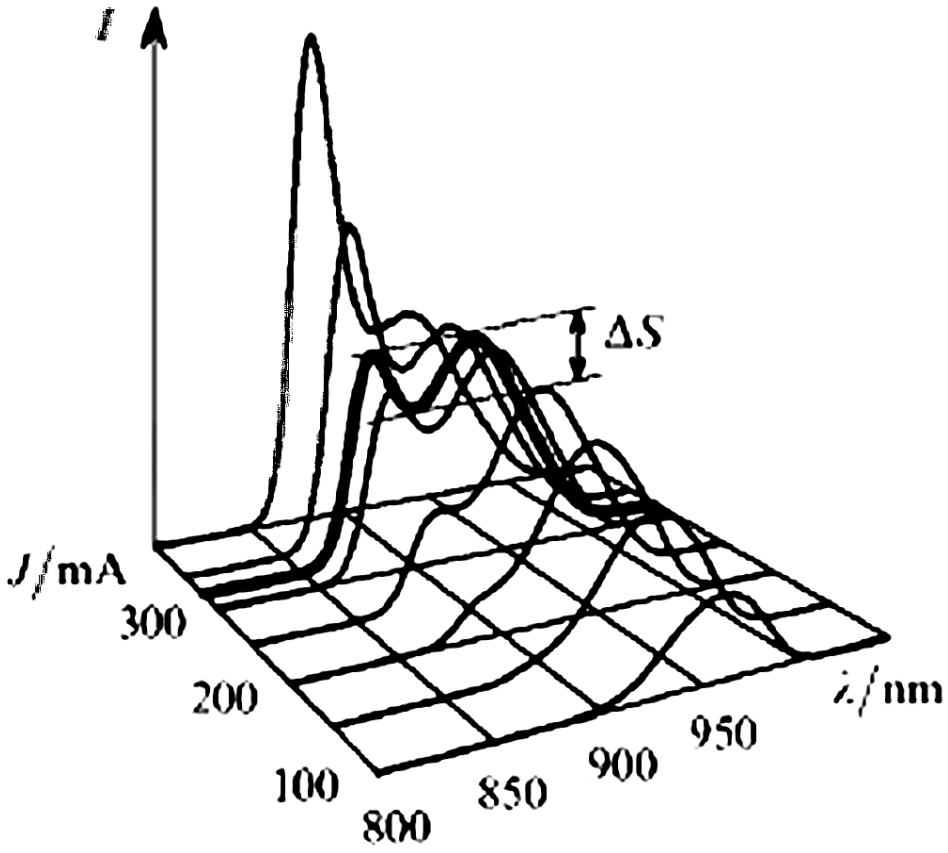

Figure 1-5. Dependence of SLD emission spectrum on injection current. As the current increases the excited state emerges. The widest bandwidth occurs when the excited state and ground state peaks are at the same intensity. Here ΔS is the distance between the bottom of the dip between the two peaks and the top of the two peaks. This dip is undesirable for OCT and can produce a ghost image. [14]

1.4 Different SLD Designs

There are several SLD designs used to achieve amplified spontaneous emission, and there are many different clever ways people are trying to achieve high power and bandwidth with SLDs. These techniques include ground state and excited state emission simultaneously, chirped quantum dots, and tapered waveguides just to name a few [4, 13, 16]

Most new SLD research takes place below or near the 1μm band, which is not an optimum band, as discussed before. A conventional two-section SLD involves the use of segmented, electrically-isolated anodes where one section acts as an absorber and the other is electrically pumped and emits light. The absorber section is reverse biased and serves to discourage feedback from the back facet of the SLD such that the device operates as a true single-pass amplifier. Another method is to use a tilted waveguide, in which the reflected light from the back facet will not enter into the waveguide due to the angle between the waveguide and back facet [17]. See Figure 1-6. This method introduces alignment complications as well as output coupling challenges in a typical optical fiber package [17]. A V-groove etch, which angles the facet, is also a method to reduce reflection from the back facet [18]. See Figure 1-6. All the techniques above are successful at suppressing the stimulated emission, but cannot solve the issue of simultaneous wide bandwidth and high power. To solve this issue different techniques to broaden the active region emission have been developed.

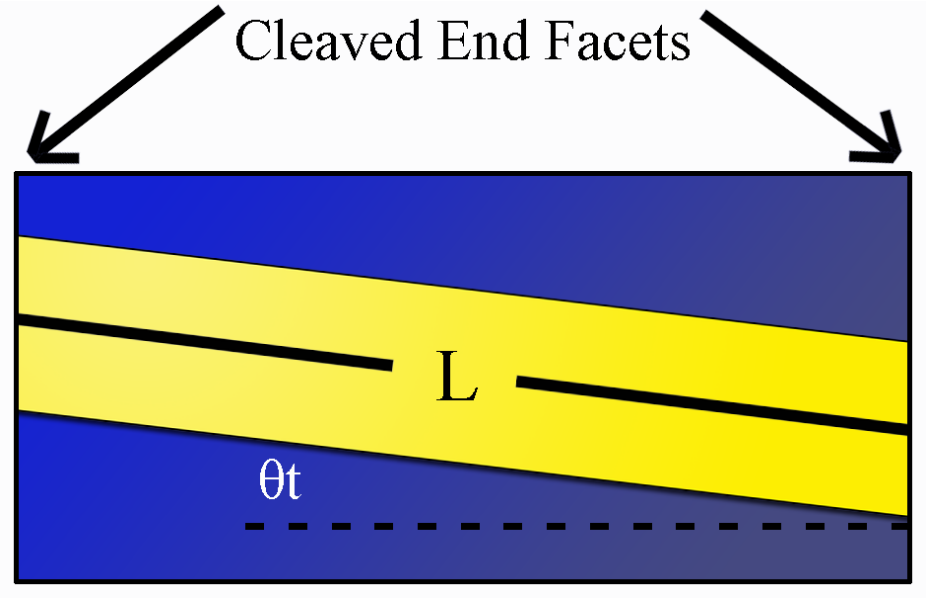

(a)

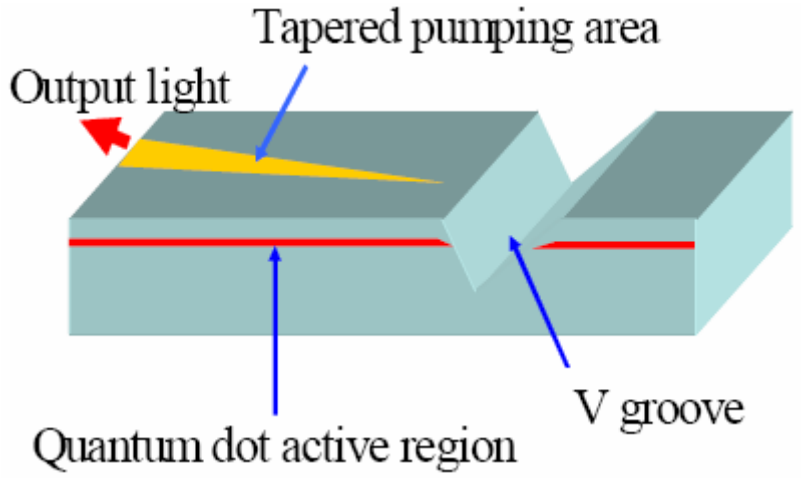

(b)

Figure 1-6. (a) top view example of a tilted waveguide, where L is the length of the waveguide and θt is the waveguide deviation angle from the normal angle to the facet (image recreated from [20]) (b) Example of a tapered waveguide and a V-groove etch (image created by Z.Y. Zhang from the University of Sheffield)

As mentioned previously, chirped quantum dots consist of multiple layers of quantum dots with each layer being tuned to a different peak wavelength. This widens the bandwidth of the emission spectrum. A SLD with chirped quantum dots, which achieved 32mW of power and a bandwidth of up to 98nm, was reported. The wavelength range covered was 1084nm to 1182nm. [13] However, there was no reported way to control the combination of the ground and excited state output emission spectra.

A tapered active region has been used to produce high power SLDs. One group has produced a SLD that emits over 200mW of power and a bandwidth of 70nm. The peak wavelengths were at 1012nm, 1036nm, and 1056nm. A tapered active region was used to increase power along with a V-groove etch to achieve low reflectivity. The active region was composed of an inhomogeneously broadened, five-layer stack of InAs-GaAs quantum dots that produced a drive-current-insensitive output spectra. However, the facet output area was 105μm [16], making it difficult to couple directly into a fiber.

Getting ground state emission and excited state emission to contribute to the bandwidth simultaneously requires their peaks to be of comparable intensities. This has been done using chirped quantum dot layers. Using tilted facets, a group achieved a bandwidth of 121nm and a power of 1.5mW under pulsed operation emitting from 1165nm to 1286nm.[4] The device power was limited to the ground state emission. As the current was increased above a certain point, the excited state takes over. The excited state intensity is fine tuned to the level of the ground state intensity; suppressing the power the excited state is capable of achieving.

A better option would be fine-tuning the intensity of the ground state to meet the intensity of the excited state emission. An ideal situation involves the excited state emission at its highest possible power, at saturation. Then the ground state emission intensity can be tuned to that same level. The device would then be emitting its highest possible power with its highest bandwidth at that power. This method is realized with the multi-section SLD design [19]. The multi-section design allows for independent adjustment of the ground state and excited state spectral bandwidth and power. This enables the realization of a wide bandwidth and high power. An OCT scan done with a multi-section SLD source can be seen in Figure 1-7.

An equation to describe the electroluminescence (EL) spectrum of the multi-section SLD has been formulated by Y.C. Xin. This equation predicts the optimized configuration for undoped and p-doped conventional InA/sGaAs quantum dot SLDs. [19] The objective of this thesis is to confirm that the multi-section SLD equation works when applied to different materials, and realize wide bandwidth with reasonable power at a center wavelength of 1.2um.

In chapter 2 the multi-section SLD will be discussed in detail. The theory behind the gain measurements and the SLD measurements will be discussed. In chapter 3 the lab test procedure will be introduced in detail and the test results will be discussed. Simulations done with the predictive equation will be presented. The consistency between theory and the actual data will show that the predictive equation is effective in simulating the emission spectrum of chirped quantum dot material.

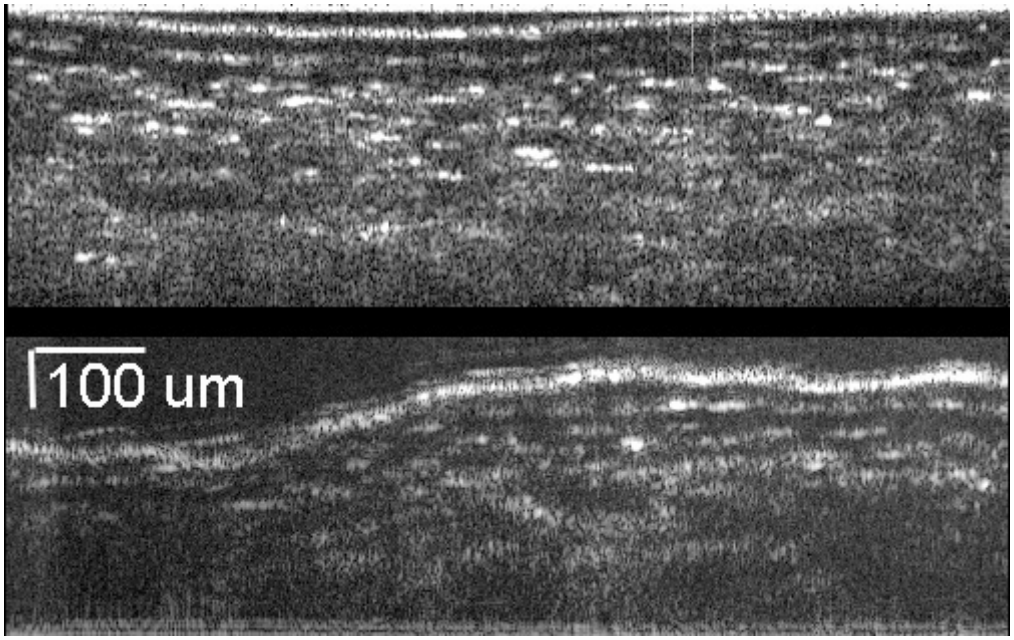

Figure 1-7. The top image is an OCT scan of onion skin using a multi-section SLD as the source. The multi-section SLD was developed by Luke Lester's group at CHTM. The bottom image is an OCT scan of an onion skin using a halogen lamp as the source. The scans were taken by Southwest Sciences.

1.5 References

[1] Yongsheng Zhao, Weihua Han, Junfeng Song, Xuemei Li, Yang Liu, Dingsan Gao, Guotong Du, Hui Cao and R. P. H. Chang, "Spontaneous emission factor for semiconductor superluminescent diodes," *Journal of Applied Physics*, vol. 85, no. 8, pp. 3945-3948, 1999

[2] Donald A. Neamen. Semiconductor Physics and Devices: Basic Principles Third Edition. New York: McGraw-Hill 2003

[3] E. Fred. Schubert. Light-Emitting Diodes. New York: Cambridge University Press, 2003

[4] L.H. Li, M. Rossetti, A. Fiore, L. Occhi and C. Velez. "Wide Emission Spectrum from Superluminescent Diodes with Chirped Quantum Dot Multilayers." *Electronics Letters* vol. 41. no.1, pp. 41-43, 2005

[5] Boppart, S. A., "Optical coherence tomography - Principles applications and advances," *Minerva Biotecnologica*, vol. 16, no. 4, pp. 211-237, 2004.

[6] Bizheva, K., Povazay, B., Hermann, B., Sattmann, H., Drexler, W., Mei, M., Holzwarth, R., Hoelzenbein, T., Wacheck, V., and Pehamberger, H., "Compact, broadbandwidth fiber laser for sub-2-μm axial resolution optical coherence tomography in the 1300-nm wavelength region," *Optics Letters*, vol. 28, no. 9, pp. 707-709, 2003.

[7] Schmitt, Joseph M. "Optical Coherence Tomography (OCT): A Review*," IEEE Journal of Selected Topics in Quantum Electronics*, vol. 5, no. 4 pp 1205-1215, 1999

[8] Wolfgang Drexler, "Ultrahigh-resolution optical coherence tomography", Journal of Biomedical Optics 9(1), pp. 47–74, 2004

[9]George Coupe, “Nanotechology: The shape of things to come,” *IEEE Manufacturing Engneer*, 2004

[10] Chun-Yen Chang, “Highlights in the Nano-World,” *Proceedings of the IEEE*, vol. 91, no. 11, pp. 1756- 1764 2003

[11] Pallab Bhattacharya, Dieter Bimbert, Yasuhiko Arakawa, “Special Issue on Optoelectronic Devices Based on Quantum Dots,” *Scanning the Issue Proceedings of the IEEE*, vol. 95, no. 9, pp. 1718-1722, 2007

[12] P. Bhattacharya, Z. Mi, “Quantum-Dot Optoelectronic Devices,” *Proceedings of the IEEE*, vol.95, no. 9, pp. 1723-1740, 2007

[13] Y. C. Yoo, I. K. Han, and J. I. Lee, “High power broadband superluminescent diodes with chirped multiple quantum dots,” *Electronics. Letters*.,vol. 43, pp. 1045–1046, 2007.

[14] D.S. Adler, T.H. Ko, A.K. Konorev, D.S. Mamedov, V.V. Prokhorov, J.J. Fujimoto, S.D. Yakubovich, “Broadband light source based on quantum-well superluminescent diodes for high-resolution optical coherence tomography,” *Quantum Electronics*, vol. 34, no. 10, pp. 915-918, 2004

[15] http://www-opto.e-technik.uni-ulm.de/lehre/cs/DOS-DIM.jpg

[16] Z. Y. Zhang, R. A. Hogg, P.Jin, T.L. CHoi, B. Xu, Z.G. Wang. “High-Power Quantum-Dot Superluminescent LED With Broadband Drive Current Insensitive Emission Spectra Using a Tapered Active Region,” *IEEE Photonics Technology Letters*, vol. 20, no. 10, pp. 782-784. 2008

[17] Yongchun Xin. Quantum Dot Multi-Section Light Emitters. Diss. University of New Mexico, Albuquerque, 2006.

[18] I. Middlemast, J. Sarma, and S. Yunns, "High power tapered superluminescent diodes using novel etched deflectors," *Electronics. Letters*., vol. 33, pp. 903–904, 1997

[19] Y. C. Xin, A. Martinez, T. Saiz, A.J. Moscho, Y. Li, T.A. Nilsen, A. L. Gray, and L. F. Lester. "1.3um Quantum-Dot Multisection Superluminescent Diodes With Extremely Broad Bandwidth," *IEEE Photonics Technology Letters*, vol.19, no.7, pp. 501-503, 2007

[20] Joseph Saizman, Raymond J. Hawkins, C.E. Zah, Serafin Menocal, and T.P. Lee, "The tilted waveguide semiconductor laser amplifier," *Journal of Applied Physics* vol. 64, no4, pp 2240-2242 1988

Chapter 2 The Multi-Section SLD

2.1 Two-Section Quantum Dot SLD

Before multi-section SLDs are discussed, it is beneficial to understand how a two-section SLD works, and its limitations. As mentioned previously, a two section SLD is a ridge waveguide edge-emitting optoelectronic device. It contains a gain section and an absorber section as can be seen in Figure 2-1(b). The front section is the gain section and emits at both the excited state and the ground state of the quantum dot active region, depending on the pump level. The back section is the absorber section, which is usually reverse-biased. If the back section is sufficiently long compared to the front section, most of the light passing through the absorber section will be significantly attenuated. However, if the absorber section is not sufficiently long, or the pump current in the front section is very high, then a reverse voltage across the absorber is necessary for the photon absorption that is needed to discourage laser action. When the quantum dot absorber section saturates (bleaches) at high pump currents, the SLD will operate as a laser. This condition, therefore, represents the upper limit on the output power of the SLD. For the quantum dot active regions investigated here, at low pump currents the emission spectrum is dominated by ground state emission. As the current density in the front section increases the first excited state emission will emerge, and will eventually dominate the emission spectrum. The widest bandwidth occurs when the ground state and excited state emission intensities are equal; however, usually this situation will not result in the highest power. Higher power occurs when the front section is pumped at

high currents, and the excited state dominates; however this yields a reduced bandwidth as depicted in Figure 2-1. With a 3-mm gain section SLD, a bandwidth of 100nm was achieved, but an output power of less than 0.1mW was produced [1]. With a higher pump current the output power could increase to 0.3mW, however the FWHM bandwidth decreased to 65nm. A high power and wide bandwidth are not easily achieved with the two-section SLD.

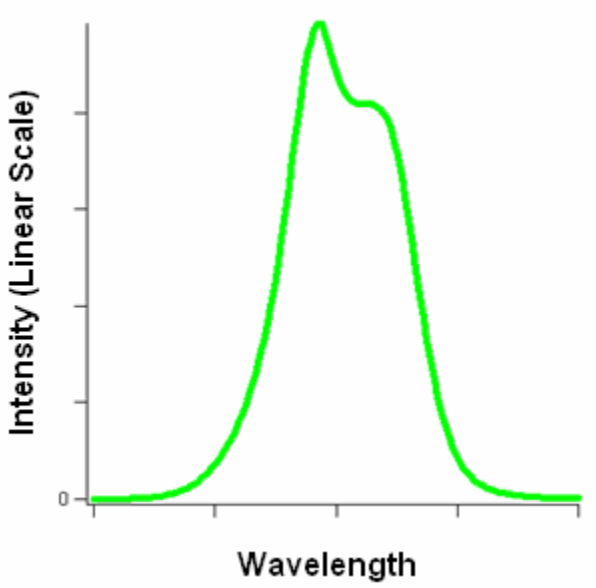

(a)

(b)

Figure 2-1 (a) Typical EL spectrum of a two-section SLD with excited state dominated emission. This results in an irregular spectrum shape. (b) Conventional two-section edge emitting SLD structure, with one gain section and one absorber section.

2.2 Multi-Section Quantum Dot SLD

The multi-section SLD design uses more than one gain section to achieve high power and wide bandwidth simultaneously as shown in Figure 2-2. In this thesis a multi-section SLD with two gain sections and one absorber section is studied. With two electrically-isolated gain sections, each section can be pumped differently. One section can be pumped at a high current density causing excited-state dominant emission, while the other gain section can be pumped at a lower current density with a ground state dominated emission spectrum as depicted in Figure 2-2. Both gain sections A_1 and A_2 amplify the spontaneous emission. For optimum results, the front gain section, A_1, that is nearest the emitting facet is pumped with a higher current density to produce excited state dominated emission, while the second or back gain section, A_2, is pumped with a much lower current density to emit ground state dominated emission.

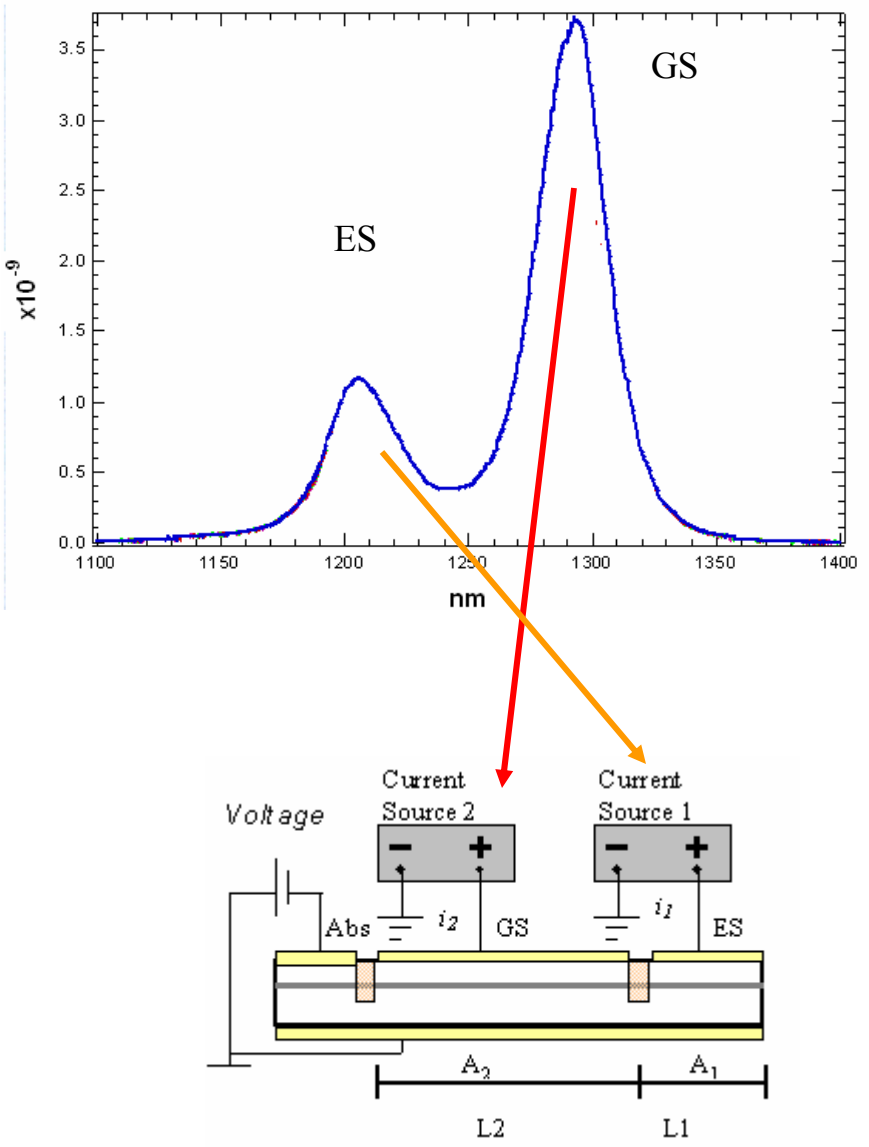

Figure 2-2. A three-section SLD with a possible EL curve, with excited state emission primarily from A_1 and ground state emission mostly from A_2. The front section is biased at a high current density and the back section is biased at a lower current density. The absorber section can be reverse biased for further photon absorption[1].

The length of each section, L_1 and L_2, as well as the pump level in each section both effect the final output spectrum of the device, as well as the gain G in each section at different current densities J_1 and J_2. The equation that describes the SLD electroluminescence spectrum is derived from the amplified spontaneous emission (ASE) intensity (I) equation below. [2]

$$I_{ASE} = (I_o + \frac{S}{G})\exp(G \cdot x) - \frac{S}{G} \qquad \text{Eqn 2-1}$$

Here I_0 is the pre-existing intensity entering the pumped region at x=0. S is the pure spontaneous emission, G is the net modal gain, and x is the position along the length of the pumped section. The net modal gain is defined by:

$$G = \Gamma g_m - \alpha_i \qquad \text{Eqn 2-2}$$

where Γ is the confinement factor, g_m is the material gain, and α_i is the internal loss. Considering the three-section SLD, which has two gain sections pumped asymmetrically, and the intensity equation (Eqn 2-1), an equation to describe the output spectrum of the this new device can be derived. The intensity I_2 produced by the back section A_2 at x=L_2, or the end of the pumped section, can be described using Eqn 2-1, where I_0 will be zero in this case because there is no intensity entering the device from the point x=0, or the edge of section A_2 nearest to the absorber.

$$I_2 = \frac{S_2}{G_2}\exp(G_2 \cdot L_2) - \frac{S_2}{G_2} \qquad \text{Eqn 2-3}$$

The intensity I_1 exiting the front section A_1 can also be described using Eqn 2-1. The intensity I_2 created by A_2 will be the starting intensity for section A_1 at point x=0.

$$I_1 = \left(I_2 + \frac{S_1}{G_1} \right) \exp(G_1 \cdot L_1) - \frac{S_1}{G_1} \qquad \text{Eqn 2-4}$$

Where I_1 is the output emission intensity of the SLD exiting A_1 at the front facet of the device. Rearranging this equation leads to:

$$I_1 = I_2 \exp(G_1 \cdot L_1) + \frac{S_1}{G_1} \exp(G_1 \cdot L_1) - \frac{S_1}{G_1} \qquad \text{Eqn 2-5}$$

Where I_2 can now be substituted, resulting in:

$$I_1 = \left(\frac{S_2}{G_2} \exp(G_2 \cdot L_2) - \frac{S_2}{G_2} \right) \exp(G_1 \cdot L_1) + \frac{S_1}{G_1} \exp(G_1 \cdot L_1) - \frac{S_1}{G_1} \qquad \text{Eqn 2-6}$$

Expanding the first term results in:

$$I_1 = \frac{S_2}{G_2} \exp(G_2 \cdot L_2) \exp(G_1 \cdot L_1) - \frac{S_2}{G_2} \exp(G_1 \cdot L_1) + \frac{S_1}{G_1} \exp(G_1 \cdot L_1) - \frac{S_1}{G_1} \qquad \text{Eqn 2-7}$$

Gathering like-terms yields:

$$I_1 = \frac{S_2}{G_2} \exp(G_2 \cdot L_2 + G_1 \cdot L_1) + \left(\frac{S_1}{G_1} - \frac{S_2}{G_2} \right) \exp(G_1 \cdot L_1) - \frac{S_1}{G_1} \qquad \text{Eqn 2-8}$$

which describes the intensity of a three-section SLD.[3] Re-writing this equation to show S and G dependencies results in the equation below.

$$I(\lambda) = \frac{S(J_2, T_2, \lambda)}{G(J_2, T_2, \lambda)} \exp[G(J_2, T_2, \lambda) \cdot L_2 + G(J_1, T_1, \lambda) \cdot L_1] + \left(\frac{S(J_1, T_1, \lambda)}{G(J_1, T_1, \lambda)} - \frac{S(J_2, T_2, \lambda)}{G(J_2, T_2, \lambda)} \right) \exp(G(J_1, T_1, \lambda) \cdot L_1) - \frac{S(J_1, T_1, \lambda)}{G(J_1, T_1, \lambda)}$$

Eqn 2-9

Here J_1 and J_2 are the injected current densities in sections A_1 and A_2, T_1 and T_2 are the junction temperatures of each section, and λ is the wavelength. The gain and spontaneous emission are both functions of current density, junction temperature, and wavelength.

Knowing the accurate gain spectra and spontaneous emission at different current densities for A_1 and A_2, a whole range of output emission spectra can be simulated by varying the lengths L_1 and L_2. Hence the optimized structures of a SLD with the best combination of power and bandwidth can be predicted without having to test a myriad of possible SLD configurations. The gain and spontaneous testing process as well as the SLD testing process can be found later in this chapter.

2.3 Design and Fabrication

If a single device is going to be tested as a three-section SLD with varying lengths for each section, then a flexible design is required. For this we use the segmented contact structure which can be seen in Figure 2-3. The multi-section SLD devices consist of a 3μm wide ridge waveguide. The ridge is divided into 500μm sections, also referred to as anodes, all electrically isolated from each other. This design allows us to vary the gain section lengths by multiples of 500μm. This can be achieved by wire bonding the desired

number of adjacent 500μm sections together, creating a single gain section. The waveguide is not tilted and the facets are cleaved. Hence the device can be tested using free-space coupling or by using a single mode fiber with a lens. The next section of the thesis describes the process flow that realizes the multi-section, segmented contact SLD.

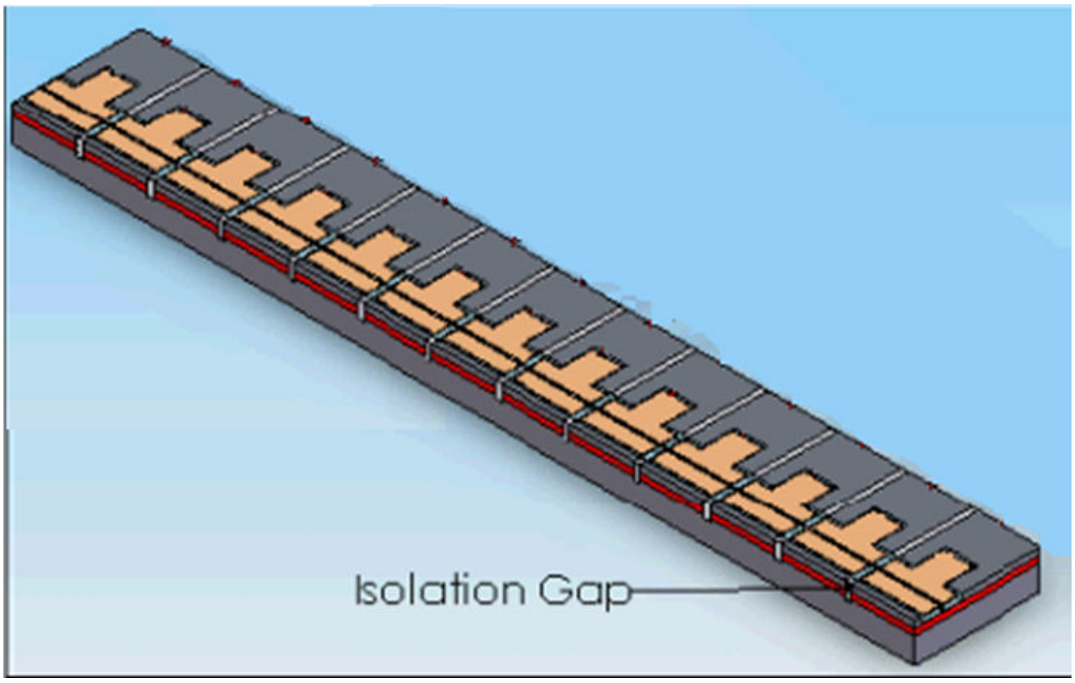

Figure 2-3. Segmented contact device structure. Each anode is 0.5mm long and is electrically isolated. They all share a common optical waveguide. They can be connected together via wire bonding in order to create desired SLD gain section lengths. This segmented contact device offers design flexibility.[1]

The wafer from which our SLD devices were made was grown by Zia Laser, Inc. ZLG 1075F was grown by molecular beam epitaxy and has 6 InAs-InGaAS dot-in-well layers with GaAs barriers. The cladding layers are $Al_{0.66}Ga_{0.34}As$. The GaAs barriers layers above the dot layers are modulated p-doped with 60 holes per dot. P-doping increases the gain. The ground state emission is centered at 1.2um.

The SLDs are processed following standard ridge waveguide processing techniques including ion implantation. The wafer is cleaned and the native oxide layer is removed. The patterning for the ridge is created on the p-side using UV contact photolithography. The mask contains several repeat device patterns to increase the yield. The ridge is etched with BCl_3 using an inductively coupled plasma (ICP) machine. The ridge is etched to just 0.1 μm above the active region to reduce current spreading and improve the optical field confinement for single lateral mode operation. Liquid BCB is evenly spun on to the surface of the wafer and baked until sufficiently hard at 250 °C. The BCB is then etched back with Oxygen and CHF_3 using a reactive ion etch (RIE) machine until the surface of the ridge is clear. The BCB filled between ridges acts as an electrical isolation layer for the p-metal after this self-alignment process. The second photolithography forms the pattern for the metal contact. The p-metal metal consisting of 500 Å titanium (Ti), 500 Å platinum (Pt), and 3000 Å gold (Au) is evaporated on to the device using an electron beam evaporator. A second metallization of Ti/Au is used to increase the p-metal thickness to at least 1 μm for good metal step coverage over the edge of the ridge where the BCB can be overetched. This thick, soft evaporated Au second metal also makes wire bonding easier. Photolithography is performed again to create the

ion implantation pattern. A thick layer of photoresist covers the entire sample with clearances at the 5 μm gaps between each 500μm section. The sample is processed using proton implantation to electrically isolate each 500μm section. This provides greater than 10 MΩ of electrical isolation. By lapping and polishing using fine-grained aluminum oxide pads, the final sample thickness is between 100μm and 200μm to ensure high quality cleave facets and sufficient thermal heat sinking. N-type metal consisting of Ge/Au/Ni/Au is then evaporated on to the back side and annealed at 380°C. Higher temperatures would crack the BCB. A simple depiction of this process is shown in Figure 2-4. The ridge waveguide devices on the sample are then cleaved in to several independent devices. The multi-section devices are mounted on an AlN chip for improved heat sinking and are ready to be tested.

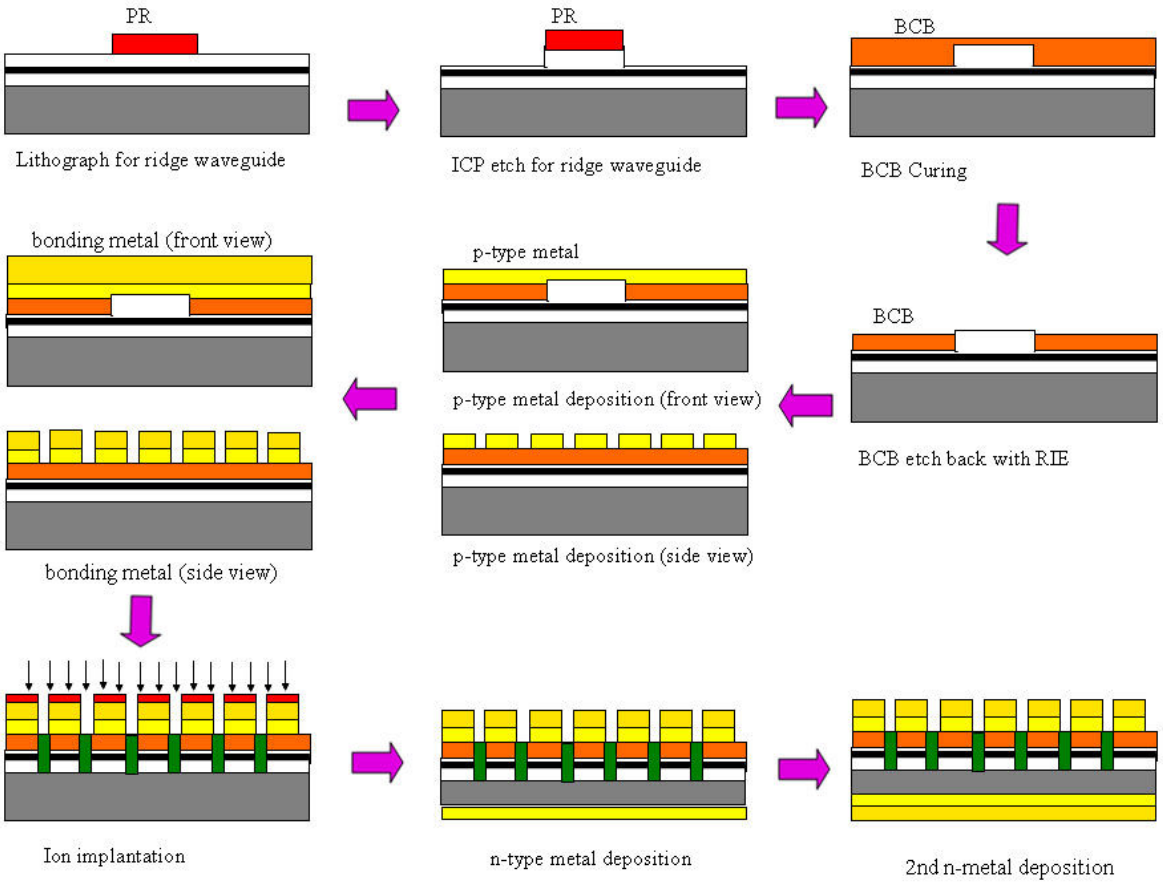

Figure 2-4. Standard process for fabricating ridge waveguide segmented contact devices. (figure recreated from [1]).

2.4 Optical Gain and Measurement

The optical gain is the fractional increase in optical mode intensity per unit distance traveled. There are different ways to measure gain of a semiconductor laser. One way is called the Hakki-Paoli technique, which determines gain by measuring the peak-to-valley ratio between longitudinal modes in a Fabry-Perot cavity below laser threshold. This technique requires a high spectral resolution to resolve longitudinal modes and is limited to current densities below the lasing threshold, which can be quite low for quantum dot active media.[4] Another method is the Henry technique, which determines gain by transforming the spontaneous emission. This method does not give the gain in absolute units.[5] A variable stripe method, which involves analyzing the spontaneous emission as a function of length, requires a constant collection efficiency and optical or electrical pumping.[6]

For this thesis, the so-called segmented contact method for measuring the optical gain was favored because it provides the gain spectrum in absolute units over a wide current range.[7,8]. The technique is based on the measurement of amplified spontaneous emission. In addition, this characterization meshes well with the multi-section layout of our SLD because the fundamental gain and absorption parameters of the active material can be tested on the actual device and then the optical circuit can be re-configured with wire bonding to fabricate the SLD.

The segmented contact method for measuring the gain and absorption as a function of wavelength normally needs only 2 sections of a known equal length to be realized. First, the section nearest the emitting facet is biased at the desired current level, and the

intensity versus wavelength is measured. This data serves as the calibrated source. Next, both sections are biased at this same desired current level. In this instance, the back section is now the calibrated source and the front section is treated as an amplifier of known length. It is straightforward then to calculate the optical gain per cm of the material. If the front section diode is reverse-biased, the resulting calculation yields the absorption of the active region. Thus, the simplicity and flexibility of the segmented contact method has made it very popular.

However, unless a rather cumbersome slit is used in front of the emitting facet the segmented contact method ignores the unguided spontaneous emission that is especially prevalent in quantum dot edge emitting LEDs. The latter occurs because QD active media have a relatively smaller optical gain than quantum well active regions. The improved segmented contact method is more appropriate for the quantum dot devices studied in this thesis [9] because it provides a cleaner and more accurate gain spectrum for QDs. The improved segmented contact method is based on the original segmented contact method but adds another section that permits background subtraction and the option of direct coupling into an optical fiber from the emitting facet. The basic difference between the improved and original segmented contact methods is how the background noise is eliminated. The original technique excludes the noise by virtue of a change in the experimental apparatus (the slit) and requires more stringent optical alignment and experimental skill. The improved version relaxes the requirements on the experimentalist and the optical alignment by making a third intensity measurement. The background noise is then subtracted out mathematically by a revised set of equations that are derived next.

The differential intensity of the amplified spontaneous emission, I_{ASE}, with transmission length, x, optical gain, G, and the pure spontaneous emission intensity, S, can be related with the equation below. [10]

$$\frac{dI_{ASE}}{dx} = GI_{ASE} + S \qquad \text{Eqn 2-10}$$

If the $I_{ASE} = 0$ at $x = 0$, the usual boundary condition, then the following equation is true. [6]

$$I_{ASE} = \frac{S}{G}(\exp(g \cdot x) - 1) \qquad \text{Eqn 2-11}$$

The unguided spontaneous emission that results from leakage current in the device or from an imperfect waveguide (I_{leak}) can induce errors in the gain data as was mentioned above. It can be related to the measured intensity as follows:[9]

$$I = I_{ASE} + I_{leak} \qquad \text{Eqn 2-12}$$

In the improved segmented contact method, the net modal gain can be analyzed from the ASE emission under three different pump configurations. The data from single, double, and triple biased sections is manipulated. First the very front section is pumped with a certain current density of J_1=J, and the ASE intensity of I_1 is measured. Next the first section is left on with the exact same J_1, but now the second section is pumped with current density J_2=J, and the intensity I_2 is measured. Next the third section is pumped with current density J_3=J, the second section with J, and the first section is still biased at

J_1. The intensity I_3 is measured. From Eqn 2-11 and Eqn 2-12, intensities I_1, I_2, and I_3 can be expressed as follows:[9]

$$I_1 = \frac{S_1}{G_1}[\exp(G_1 L) - 1] + I_{leak1}$$
$$I_2 = \frac{S}{G}\exp(G_1 L)[\exp(GL) - 1] + \frac{S_1}{G_1}[\exp(G_1 L) - 1] + I_{leak2} \qquad \text{Eqn 2-13}$$
$$I_3 = \frac{S}{G}\exp(G_1 L)[\exp(2GL) - 1] + \frac{S_1}{G_1}[\exp(G_1 L) - 1] + I_{leak3}$$

In the equations above, G_1 corresponds to the net modal gain when the section is biased with J_1 and G corresponds to the net modal gain when a section is biased with J. The usual experimental condition is $J_1=J_2=J_3=J$, but the more general form of Eqn 2-13 allows for more flexibility in allowing the source term I_1 to differ from the amplifier sections.

The unguided spontaneous emission exiting from sections 2 and 3 will primarily radiate out of the optical waveguide and never make it to the coupling lens, leaving section 1 the dominant source for unguided spontaneous emission. If we assume that the total I_{leak} is the same for the different pumping configurations, mathematically that $I_{leak1}=I_{leak2}=I_{leak3}$, then we can say [9]

$$G = \frac{1}{L}\ln(\frac{I_3 - I_1}{I_2 - I_1} - 1) \qquad \text{Eqn 2- 14}$$

The unguided spontaneous emission terms cancel out in Eqn 2- 14. Hence the improved segmented contact method has the ability to measure small gain values

accurately. This improved segmented contact method was tested for accuracy two different ways. First the gain with 1-mm long sections was extracted and the gain with 1.5-mm long sections was extracted, both using the same current density. It was verified that the gain from both lengths corresponded very nicely. Next a self-calibrating method was used to verify the accuracy. The device was made to act like a laser, and the gain data was derived from the threshold condition at a certain wavelength. The gain at the threshold current density was taken using the segmented contact method as well. The two gains corresponded nicely to an accuracy within 0.1 cm^{-1}.

2.5 Unamplified Spontaneous Emission

From Eqn 2-13 it is evident that the optical gain and unamplified spontaneous emission at specific current densities, as well as section lengths, must be gathered before the intensity of the SLD can be predicted. Lengths are something that can be chosen, and the improved segmented contact method was introduced as a method to measure optical gain. All that needs to be addressed is a mathematical expression for the unamplified spontaneous emission in terms of the measureable quantities in the improved segmented contact method. Using Eqn 2-13 and assuming I_{leak} is the same for I_1, I_2, and I_3, a relationship between I_{ASE}, the net modal gain, and unamplified spontaneous emission is given by:

$$I_2 - I_1 = \frac{S}{G}[\exp(G \cdot L) - 1]\exp(G \cdot L) \qquad \text{Eqn 2-15}$$

This can be re-arranged to produce an equation relating the unamplified spontaneous

emission S in terms of G, L, and I_1 and I_2.

$$S = G\frac{I_2 - I_1}{(\exp(G \cdot L) - 1)\exp(G \cdot L)} \qquad \text{Eqn 2-16}$$

A detailed testing procedure for the SLD measurements and the gain measurements can be found in the next chapter, as well as SLD emission simulations from the gain measurements using Eqn 2-9.

2.6 Summary

The purpose of this project was to realize a SLD device with a peak emission wavelength of 1200nm, a bandwidth of at least 100nm with a dip less than 3dB, and a reasonable output power. The dip between the excited state and the ground state emissions is undesirable for OCT and can produce a ghost image or double image. In this chapter the basic two-section SLD design was discussed, and its shortcomings were revealed. The multi-section SLD design was shown to provide high power and the ability to achieve a wide bandwidth by aligning the excited state peak emission with the ground state peak emission. An equation used to predict SLD electroluminescence spectrums was discussed. The improved segmented contact method was introduced as the best way to measure gain for quantum dot ridge-wave guided devices due to its ability to cancel noise created from unguided spontaneous emission. A way to extract unampified spontaneous emission was also discussed.

2.7 References

[1] Yongchun Xin. Quantum Dot Multi-Section Light Emitters. Diss. University of New Mexico, Albuquerque, 2006.

[2] Joseph T.Verdeyen, Laser Electronics 1995.

[3] Y. C. Xin, A. Martinez, T. Saiz, A.J. Moscho, Y. Li, T.A. Nilsen, A. L. Gray, and L. F. Lester. "1.3um Quantum-Dot Multisection Superluminescent Diodes With Extremely Broad Bandwidth," *IEEE Photonics Technology Letters*, vol.19, no.7, pp. 501-503, 2007.

[4] B.W. Hakki, T. L. Paoli, " Gain Spectra In GaAs Double-Heterostructure Injection Lasers*," Journal of Applied Physics*, vol. 46, no. 3, pp. 1299- 1306, 1975

[5] C. H. Henry, R. A. Logan, F. R. Merritt, "Measurement of Gain and Absorption-Spectra in AlGaAs Burried Heterostructure Lasers," *Journal of Applied Physics*, vol. 51, no. 6. pp. 3042-3050, 1980

[6] A. Oster, G. Erbert, H. Wenzel, "Gain Spectra Measurements by a Variable Stripe Length Method with Current Injection," *Electronics Letters*, vol. 33, no. 10, pp. 864-866, 1997.

[7] J. D. Thomson, H. D. Summers, P. J. Hulyer, P. M. Smowton, and P. Blood, "Determination of single-pass optical gain and internal loss using a multisection device," *Applied Physics Letters*, vol. 75, no. 17, 2527-2529, 1999

[8] P. Blood, G. M. Lewis, P. M. Smowton, H. Summers, J. Thomson, and J. Lutti, "Characterization of semiconductor laser gain media by the segmented contact method,"*IEEE Journal of Selected Topics in Quantum Electronics*, vol. 9, no. 5, pp. 1275-1282, 2003.

[9] Xin, Y. C., Li, Y., Martinez, A., Rotter, T. J., Su, H., Zhang, L., Gray, A. L., Luong, S., Sun, K., Zou, Z., Zilko, J., Varangis, P. M., and Lester, L. F., "Optical gain and absorption of quantum dots measured using an alternative segmented contact method," *IEEE Journal of Quantum Electronics*, vol. 42, no. 7-8, pp. 725-732, 2006.

[10] J. T. Verdeyen, Laser Electronics. Englewood Cliffs, NJ: Prentice Hall, 1995

Chapter 3 - Testing Procedure and Results

3.1 General SLD measurement process

There are many possible SLD configurations with many different current densities that can be tested. For any given configuration, maximum power and bandwidth are desired. To reduce the amount of test options, the saturated power for possible lengths of the front section L_1 is measured and L_1 is biased at its saturation current density during SLD measurements. It has been determined in the past that the optimum configuration for a SLD with two gain sections has the length of amplifier A_1about half the length of A_2. The entire cavity length of the device is considered, and A_1 and A_2 are divided such that the ratio of L_1 to L_2 is about ½. Intensity measurements used to extract gain, which are referred to as Gain measurements in this chapter, are taken at the A_1 saturation current density, as well as a wide range of lower current densities for A_2. Once all desired intensity measurements are taken there is enough data to begin extracting gain spectra, then the unamplified spontaneous emission can be extracted as well. With the gain and spontaneous emission spectrums available, the predictive SLD equation (Eqn 2-9) can be used to create theoretical SLD electroluminescence curves. Several curves can be generated. Power measurements are then taken for different SLD configurations, and a graph comparing bandwidth and power can help identify configurations with a combination of optimum power and bandwidth. Next, SLD EL measurements can be taken for the configurations that theoretically yield desirable results. In this thesis only CW pump conditions are used.

3.2 Saturated Power Test Procedure and Results

First the desired devices must be separated from the larger wafer sample. After the desired sample is made independent, and the desired length is chosen, the end facets are cleaved, creating a smooth facet with 32% reflectivity. The device is mounted n-side down on to a copper heat sink using indium. The sample is then placed on copper submount that is bonded to a thermoelectric (TE) cooler. The TE cooler is used to hold the temperature at 28°C, which is a realistic operating temperature for a SLD. The device is probed with a special probing apparatus that contains several independent tiny probes. Each probe is electrically isolated and hooked up to an ILX Lightwave LDC 3916 16-channel Laser Diode Controller through a 16-probe card. Each needle has a diameter of 0.75mm and is connected to one of the bond pads on the device as seen in Figure 3-1 below. The total current is monitored with a multi-meter. The device is positioned so that one facet hangs over (less than 50μm) the edge of the copper to prevent reflections from the copper.

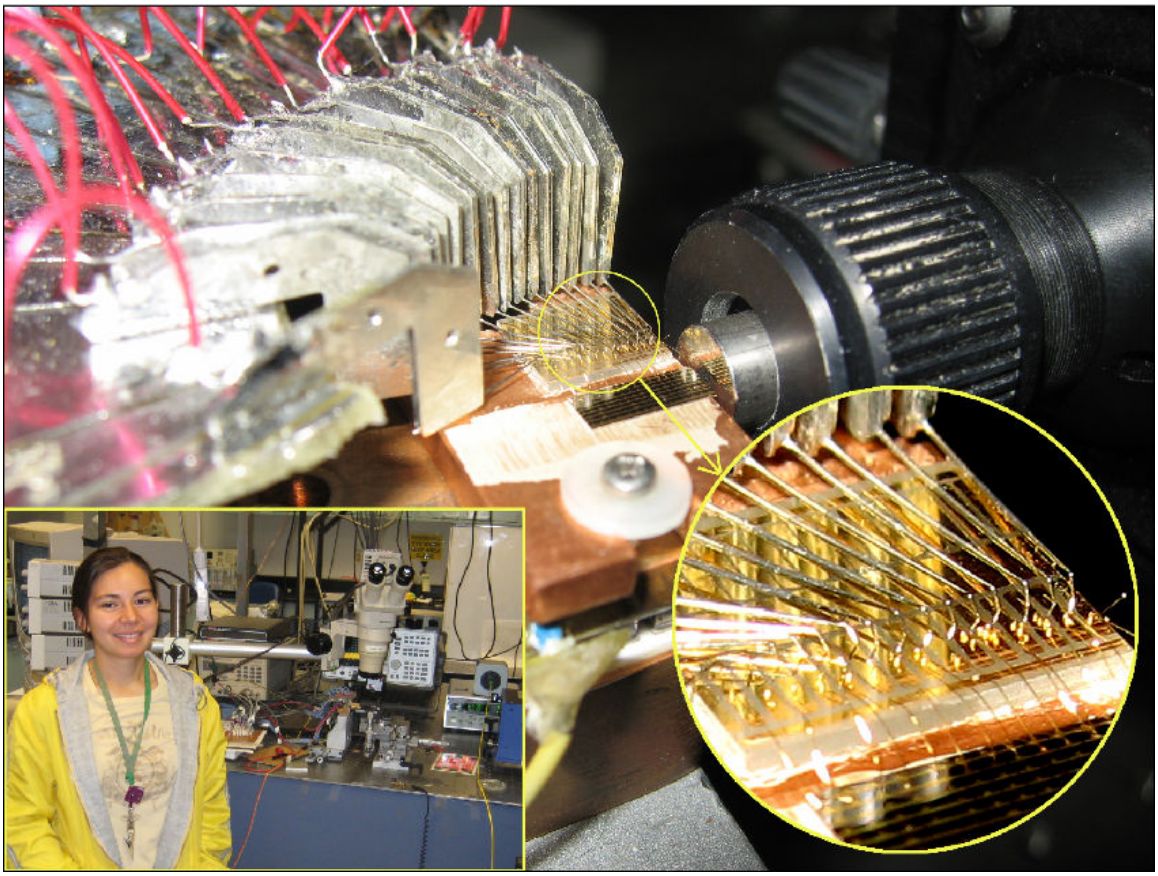

Figure 3-1. Device Probing Setup. Several electrically isolated probes are used to contact each electrically isolated anode.

The saturated power of the first few sections is found, and A_1 is biased at the current density associated with this saturated or maximum power. If A_1 is biased at a current density higher than that of the saturation current density then heating is increased and a red shift occurs, and there is no increase in power. Finding the saturated power is done with an integrating sphere (Labsphere brand) that can capture all of the light from the large beam divergence SLD. The Labsphere is positioned in front of the facet, with the facet pointing directly into the back of the Labsphere. The 16-channel current source contains a GPIB card that allows it to be controlled remotely by a computer. An Igor Pro computer program is used to control the source and set the current in each probe. The data from the Labsphere can also be extracted using Igor Pro. To find the saturated power, the desired section length is chosen in Igor, and the current is set to scan in the desired probes. For the purpose of finding the saturated power, the current is scanned in the first 500μm section and the current near the saturated power is noted. This is done with a 1-mm long section, and then a 1.5-mm long section, and finally 2-mm long section. The setup can be seen in Figure 3-2 and the results can be seen in Figure 3-3. For the 2-mm long device the power saturates at about 180mA per 500μm section.

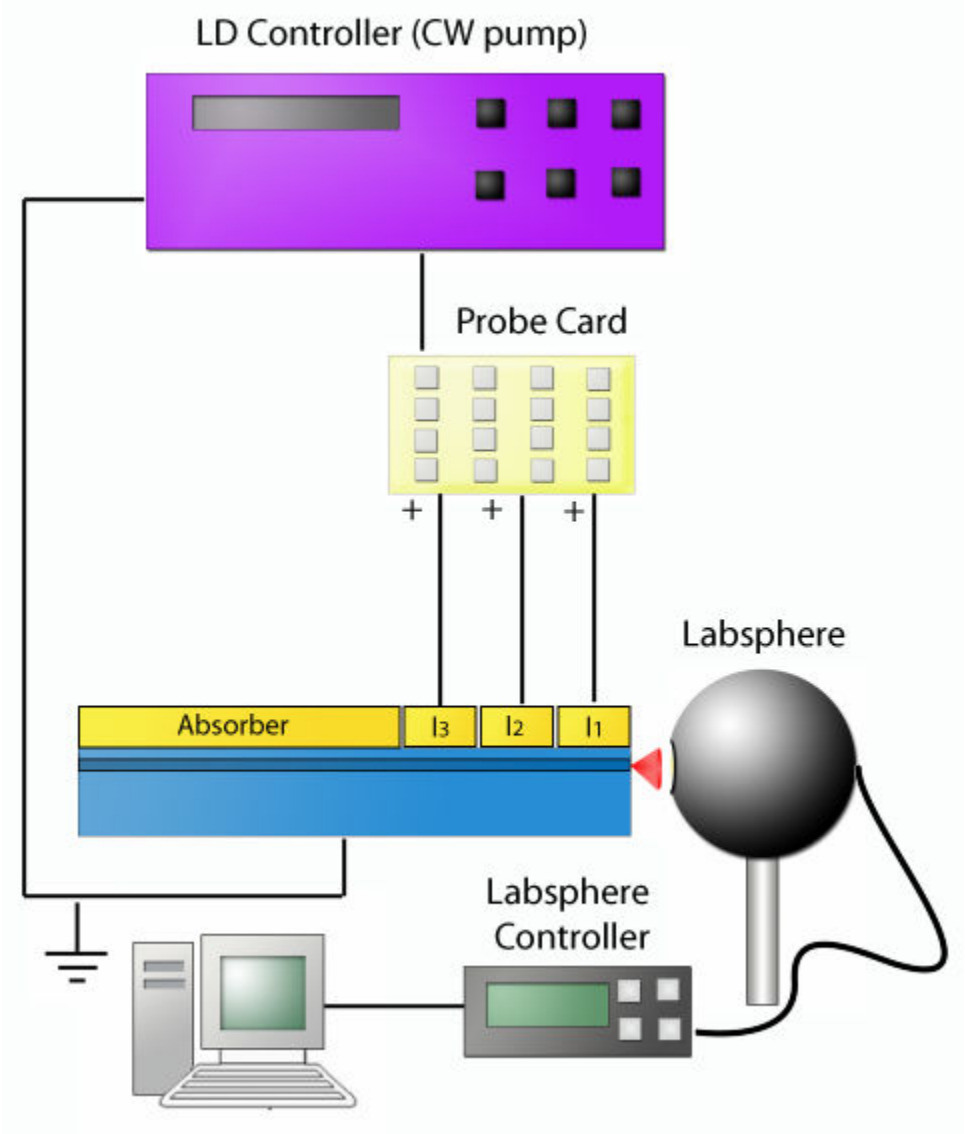

Figure 3-2. Power measurement setup. This setup involves a laser diode controller, a probe card, a labsphere, and a computer to record the data.

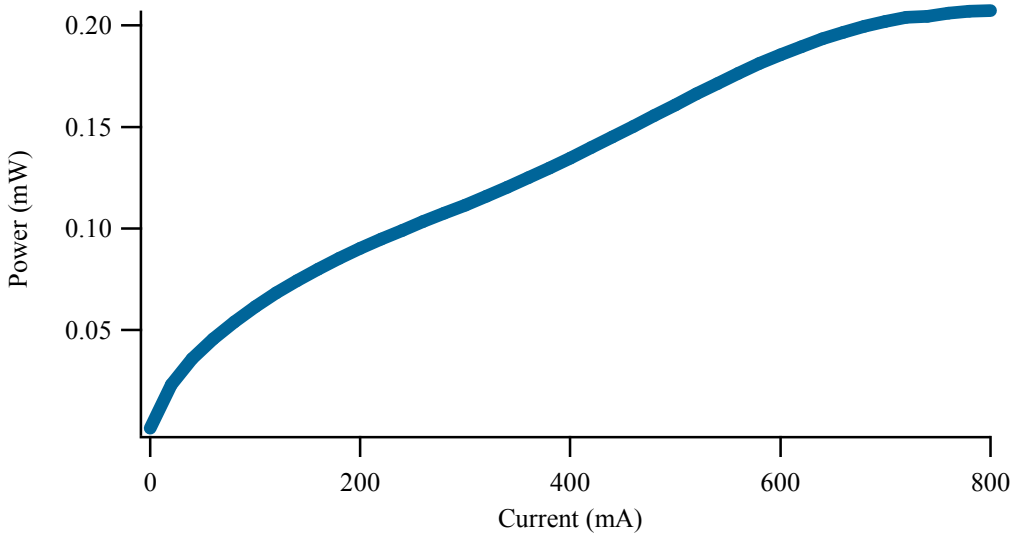

Figure 3-3. L-I curve for a 2-mm long section. The power saturates between 700 and 750mA, or at about 180mA per 0.5-mm long section.

3.3 Gain Measurement Procedure and Results

The theory for measuring gain was described in Chapter 2. In this section the lab testing procedure for measuring gain is discussed. The Labsphere from the previous test is removed from the setup, and an optical head consisting of a lens, isolator and fiber pigtail is placed directly at the front facet. The fiber is hooked up to a power meter initially for alignment. The maximum coupling efficiency is 40%. The probes were all activated, and equal current was distributed to each 500μm section. With each section being pumped with equal current the device acts as a laser and alignment is easily done above the threshold. After good alignment is achieved the power meter is removed and the end of the fiber is now connected to an Agilent 86142B Optical Spectrum Analyzer. The resolution is set to 1nm and the averaging is set to 10. The setup can be seen in Figure 3-4. Everything is now set up properly to begin taking measurements for intensities I_1, I_2, and I_3. For our purposes there is no need to pump the first section with a different current density than the other two sections as was generally described in Eqn. (2-13). The first section is pumped with the desired current density J and I_1 is measured. Then the first and second sections are each simultaneously pumped with the same current density J and I_2 is measured. Then all three adjacent sections are simultaneously pumped with the same current density J and I_3 is taken. One set of I_1, I_2, and I_3 EL spectra can be seen in Figure 3-5. In this particular device there is 5mm of un-pumped device to act as an absorber so there is no back reflection interfering with the measurements. This process was repeated for currents from 4mA to 10mA. The gain was extracted from the data taken using Eqn 2-14, where L in this case is 500um. This data is taken in order to

simulate ground state emission from the second gain section. The results can be seen in Figure 3-6. There is gain only for the ground state in these gain graphs. For some current densities it appears as though there is no gain at all. This loss is due to the gain section acting like an absorber at low current densities. For a 2-mm long section the power saturates at about 180mA/section, so gain measurements were taken at 180mA/section. This data is taken at such a high current density to simulate the excited state emission from the front gain section using Eqn 2-9. The results are in Figure 3-6. We can see from this figure that there is gain in both the ground state and excited state. The unamplified spontaneous emission curves are also extracted from this data using Eqn 2-16.

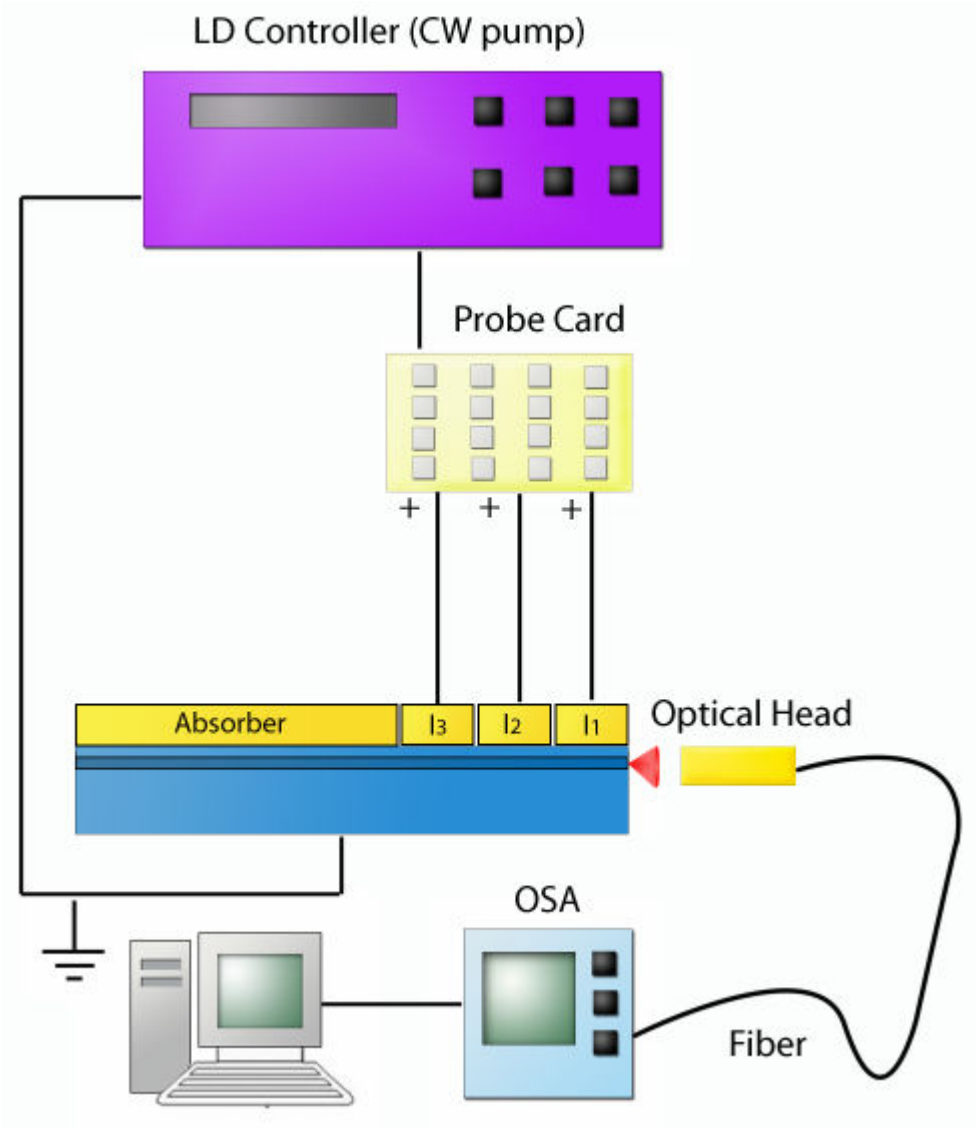

Figure 3-4 Gain measurement setup. This setup include a laser diode controller, a probe card, an optical head connected to a single mode fiber, an optical spectrum analyzer, and a computer to record the data.

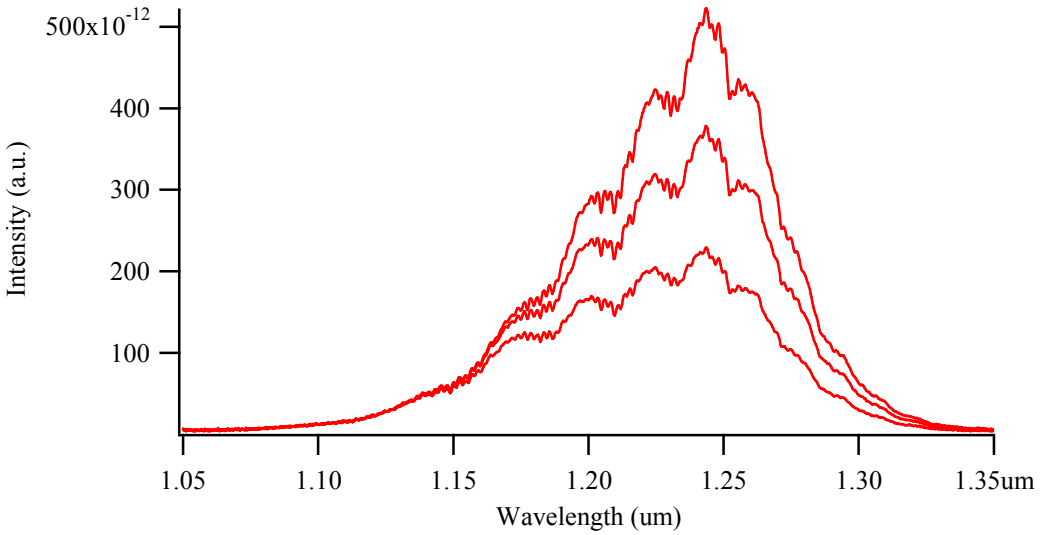

Figure 3-5. EL Curves for I_1, I_2, and I_3 at 5mA per 0.5-mm long section. Gain and spontaneous emission spectra are calculated from measured I_1, I_2, and I_3 spectra.

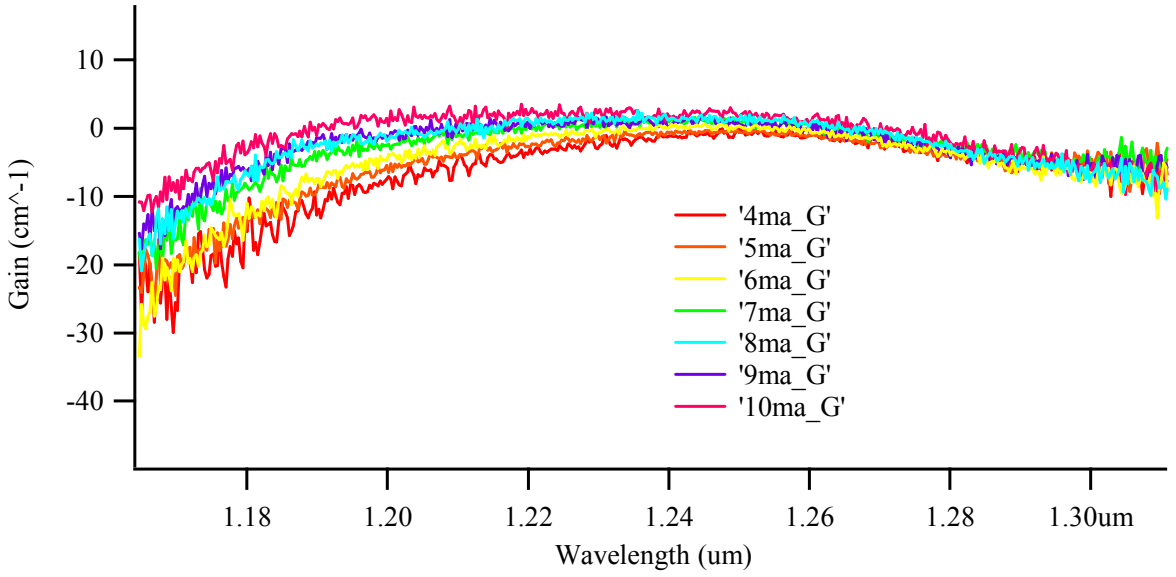

(a)

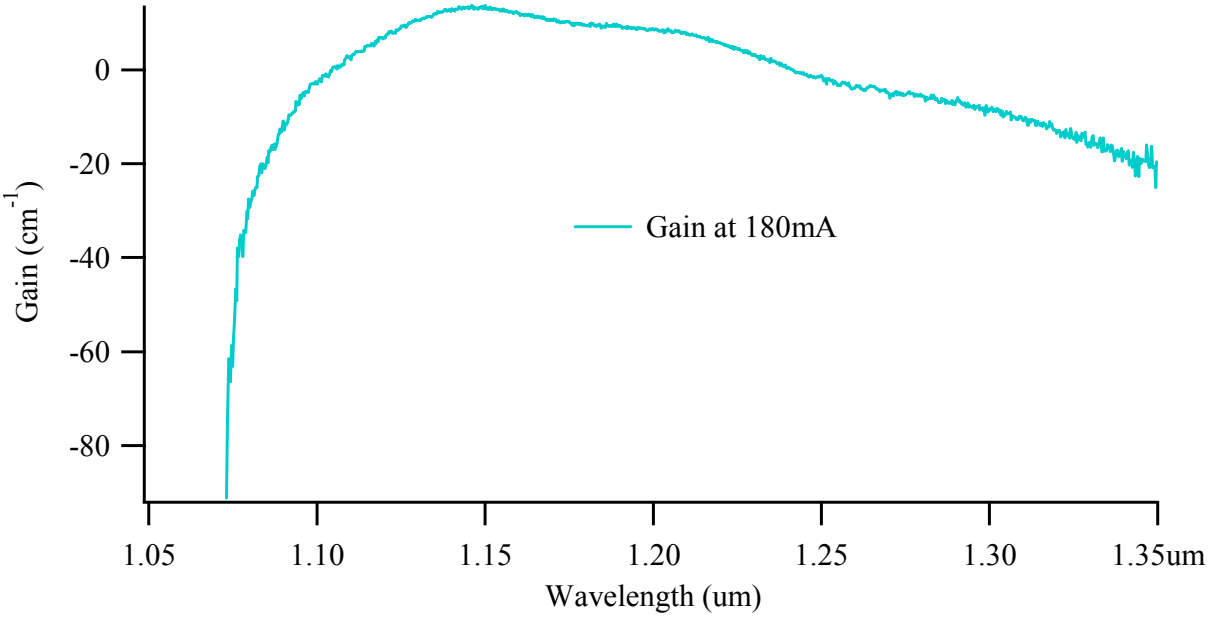

(b)

Figure 3-6. Extracted gain measurement for (a) lower current densities 4mA - 10mA/0.5mm long section (b) and at 180mA/0.5mm long section

3.4 Simulations

With the SLD predictive equation (Eqn 2-9), theoretical SLD EL spectrums for many configurations with different pump currents can be generated. The configurations at current densities which yield the highest bandwidth can be determined. At this point in the testing all the data that is needed to create a simulated EL SLD spectrum is available. Several simulations were done. The first was done with an L_1 of 0.5mm and a varied L_2. Simulations with an L_1 of 1mm were done, while L_2 was varied. It has been demonstrated that the widest bandwidths occur when L_2 is roughly twice the length of L_1. For this reason, only theoretical configurations where L_2 is about twice L_1 were simulated. This process was repeated for L_1 being 1.5mm, 2mm, and 2.5mm. The results can be seen in Figure 3-7 and Figure 3-8. The higher bandwidths result in the shorter overall cavity length. As the total cavity length L_1+L_2 becomes larger, the bandwidth decreases. It is evident from Table 3-1 that as L_1 increases the maximum bandwidth for each different L_1 length decreases.

1st Section Length (**L1**)	2nd section Length (**L2**)	Bandwidth (3-dB)
0.5mm	1mm	148nm
	1.5mm	142nm
	2mm	132nm
1mm	1.5mm	144nm
	2mm	148nm
	2.5mm	134nm
1.5mm	2mm	114nm
	2.5mm	113nm
	3mm	123nm
	3.5mm	124nm
2mm	3mm	97nm
	3.5mm	101nm
	4mm	104nm
	4.5mm	104nm
2.5mm	4mm	90nm
	4.5mm	94nm
	5mm	93nm
	5.5mm	91nm

Table 3-1. Simulation Table: Includes lengths L_1 and L_2 and the widest simulated bandwidth for each configuration. As the length of L1 increases the widest achievable bandwidth decreases.

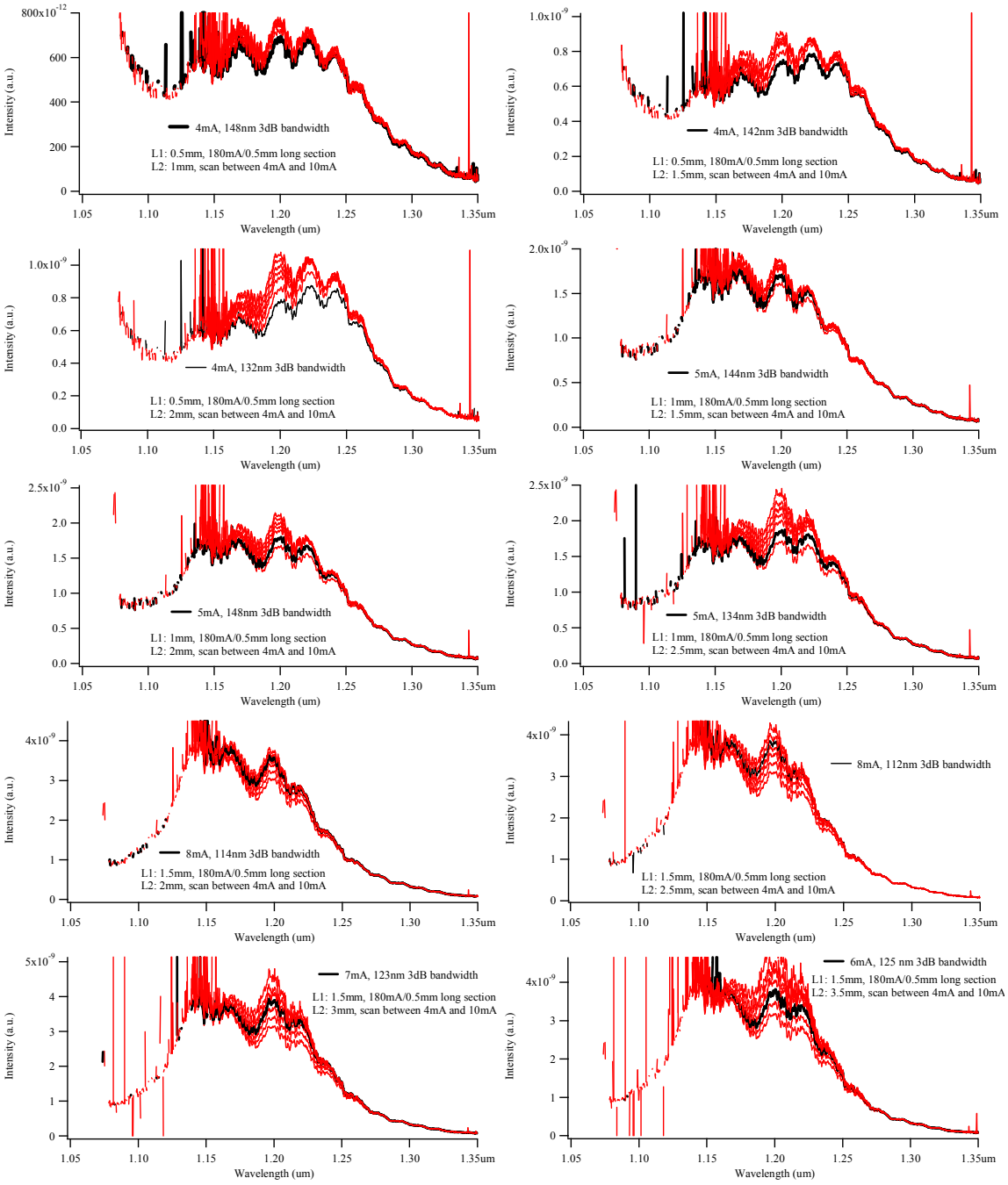

Figure 3-7. Simulation results for A1 section length of 0.5mm, 1mm, and 1.5mm, with varying lengths for A2. The black curve is the widest bandwidth for each particular SLD configuration. Each curve is simulated with a front section biased at 180ma/0.5mm long anode, and a second gain section biased from 4ma-10ma/0.5mm long anode.

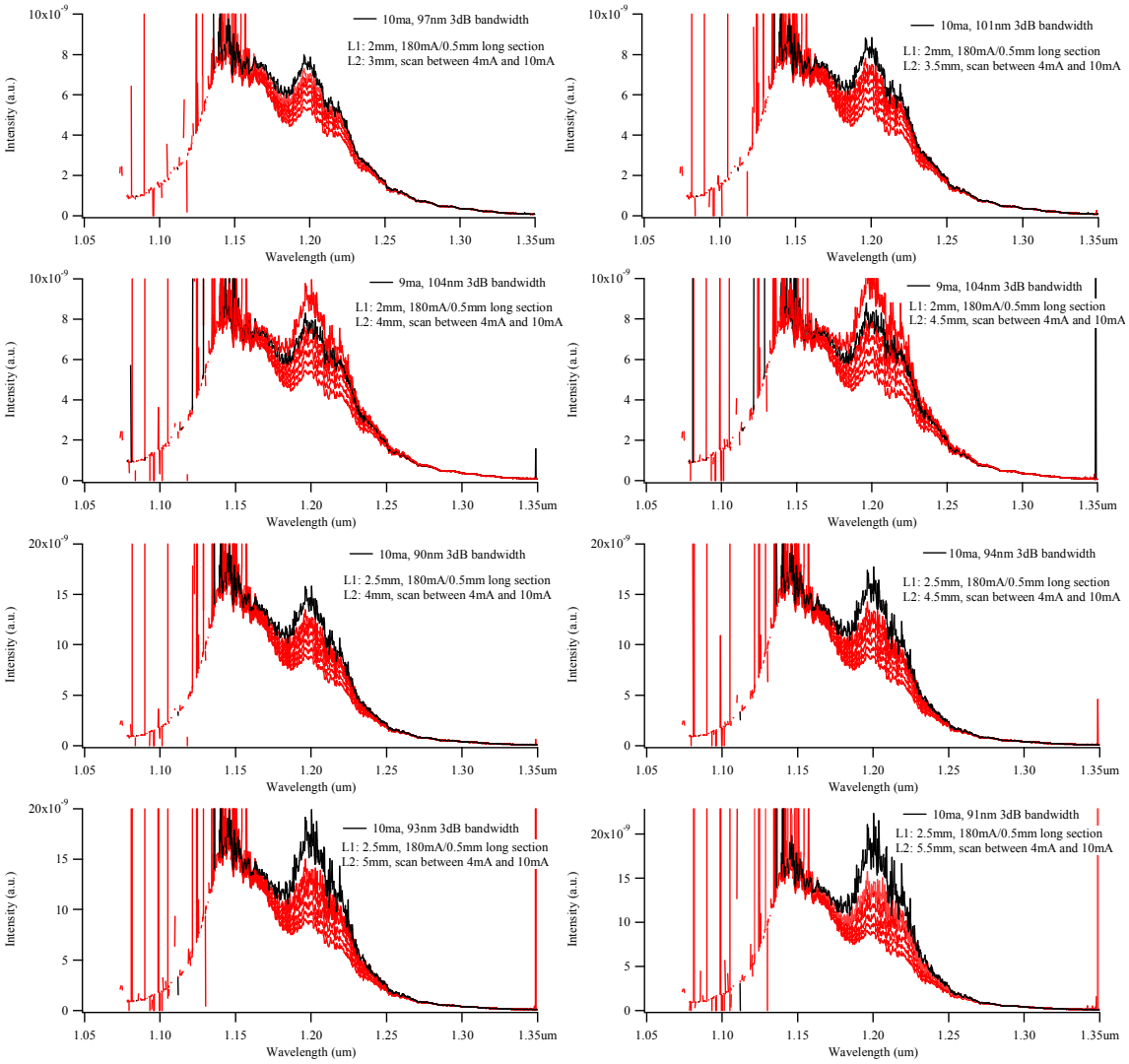

Figure 3-8. Simulation results for an A_1 length of 2mm and 2.5mm, with varying lengths for A2. . The black curve is the widest bandwidth for each particular SLD configuration. Each curve is simulated with a front section biased at 180ma/0.5mm long anode, and a second gain section biased from 4ma-10ma/0.5mm long anode.

3.5 SLD Measurements Procedure and Results

The theory for measuring a SLD EL spectrum was described in Chapter 2. In this section the lab testing procedure for measuring the SLD EL spectrum is discussed. The 16-channel laser diode controller was used to control the current to each 500-um section. Each SLD configuration of interest was achieved by designating sections for A_1 and A_2 in Igor, and then controlling the desired current densities to each section using Igor and the 16-channel current source. The theoretical SLD power was calculated using the slope efficiency extracted from Figure 3-3. Both simulated power and simulated bandwidth versus front gain section length are plotted on the same graph in Figure 3-9. As L1 increases the power also increases, however the bandwidth decreases. For this project a bandwidth of 100nm is desired. This is achievable for an L1 of 0.5mm to 2mm. The power is above 0.2mW at an L1 of 2mm and 2.5mm. This power is reasonable for OCT. An L1 of 2mm meets both the power and bandwidth requirements of this project so this length was chosen for SLD testing.

The setup used to measure the SLD EL spectrum is similar to that of the gain measurement setup and can be seen in Figure 3-10. The SLD is aligned to an optical head attached to a single mode fiber which is connected to an OSA. SLD measurements were taken with an L_1 of 2mm. The length of L_2 was varied and the current density was also varied. A reverse-bias voltage of -4 volts was placed across the absorber section, which varies in length according to the different SLD configurations. For the device used in this thesis the total device length is 7.5 mm. The back facet was destroyed to further discourage laser action by reducing reflections. The results can be seen in Figure 3-11.

The SLD EL testing with an L_1 of 2mm and an L_2 of 4mm produced two curves with an excited state peak and ground state peak at about the same intensity. A bandwidth of 111nm and a power of 0.25mW were obtained for 180ma/section injected into A_1 and 9ma/section injected into A_2 as seen in Figure 3-11 (a). A bandwidth of 111nm and a power of 0.24mW were measured for 180ma/section injected into A_1 and 8ma/section injected into A_2 as can be seen in Figure 3-11 (b). The SLD EL testing with an L_1 of 2mm and an L_2 of 4.5mm yielded a bandwidth of 118nm and a power of 0.224mW for 180ma/section injected into A_1 and 8ma/section injected into A_2 as can be seen in Figure 3-11 (c). Plotting both the calculated and actual tested SLD EL spectra on the same graph, it can be seen that calculated shape and size for each spectrum are in good agreement with their corresponding actual measured data. The measured SLD spectra are all slightly red shifted. This most likely is caused from device heating. One problem with the calculated data is the noise in the shorter wavelength range and number of points that are missing from the shorter wavelength range. The simulated curves are point to point calculations from the actual I_1, I_2, and I_3 spectra. The noise in the calculated spectra is caused by the noise in the actual data at those shorter wavelengths. The gain is weak in the shorter wavelength range.

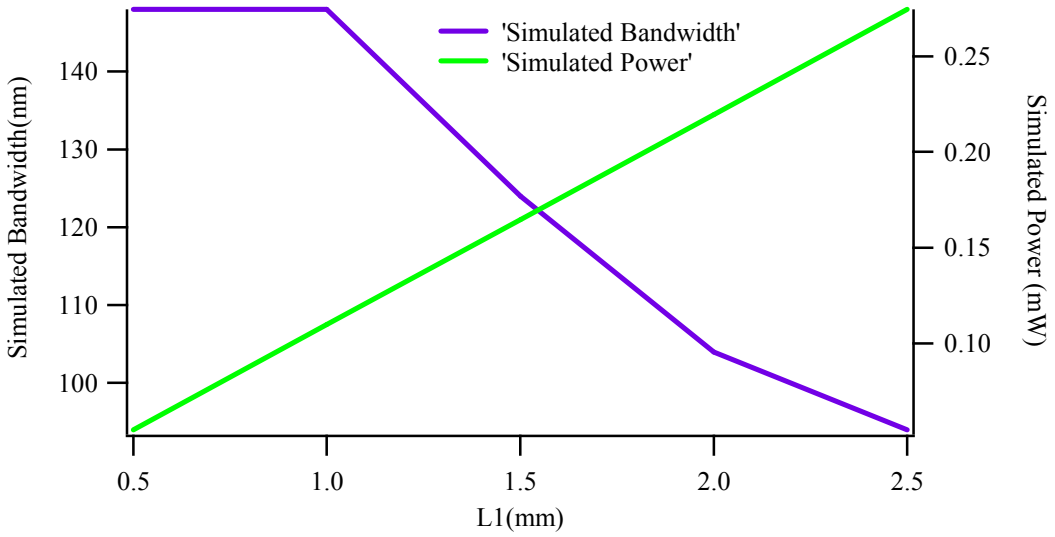

Figure 3-9. SLD simulated power versus the L_1 length compared to the SLD simulated bandwidth versus L_1 length

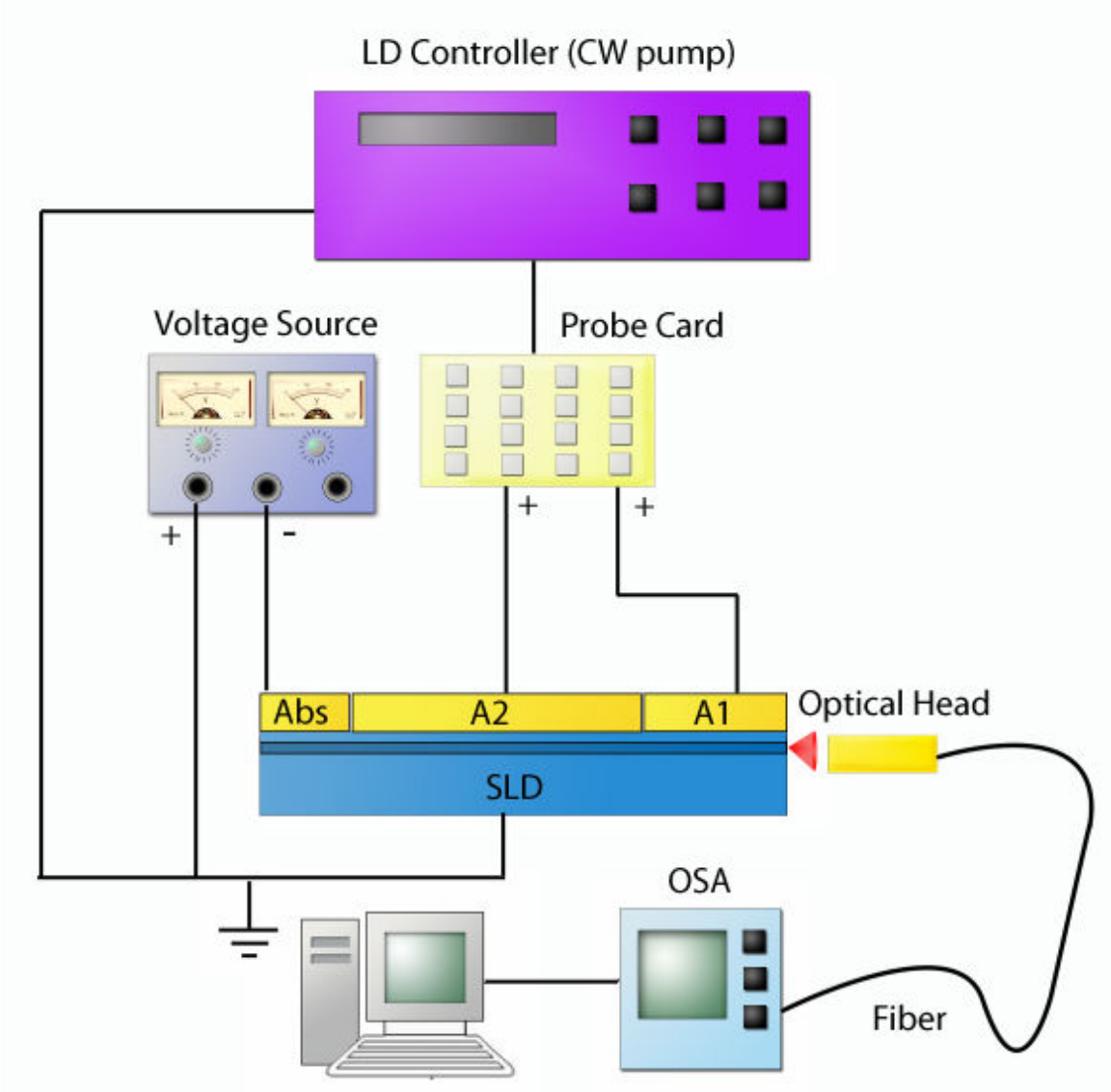

Figure 3-10. SLD EL curve measurement setup

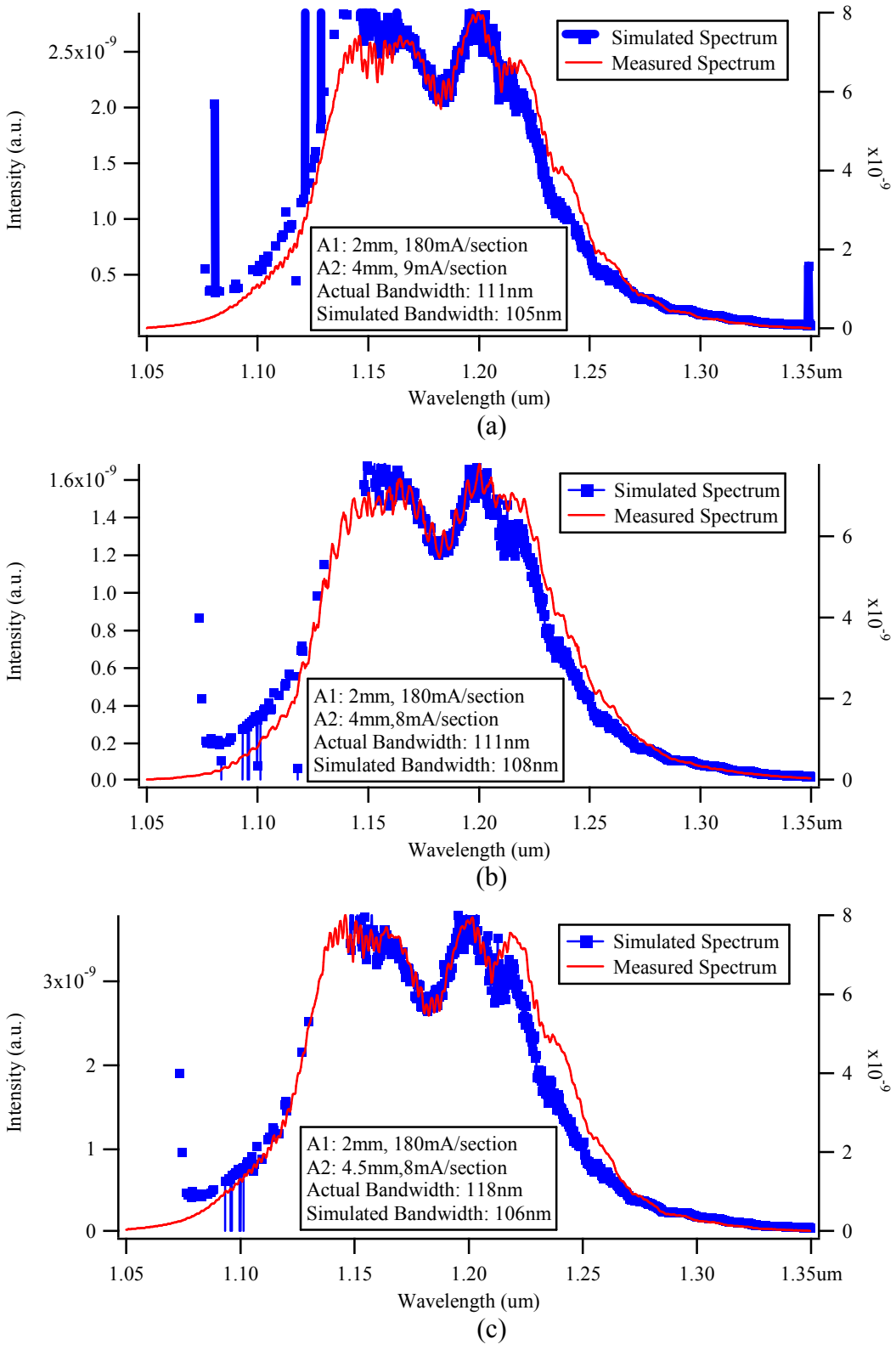

Figure 3-11. SLD EL spectrum measurements (red) compared to the simulations with the same configuration and current density(blue)

3.6 A Simulation Alternative for the SLD Spectrum

To reduce the noise in the simulation demonstrated in the previous section, the improved segmented contact method intensity spectrums I_1, I_2, and I_3 were curve-fitted using polynomial fits, each spectrum using a different number of terms to achieve the best fit. The curve fitted intensity spectrums were then substituted into the gain equation (Eqn 2-14) and the spontaneous emission equation (Eqn 2-16), and the resulting spectrums were plugged in to the predictive SLD intensity equation (Eqn 2-9). The improved segmented contact intensity spectrums for 8ma and 180ma were curve-fitted in this way and the coefficients can be seen in Table 3-2. This produces a calculated SLD intensity spectrum with a front gain section (A_1) pumped at 180ma/0.5mm section and a second gain section (A_2) pumped at 8ma/.5mm section. The length of A_1 was chosen to be 2mm and the length of A_2 was chosen to be 4mm. The resulting SLD EL spectrum is not in good agreement with the actual data or the SLD EL spectrum calculated from the actual data I_1, I_2, and I_3. This is most likely due to the error in the curve fitting. The error produced by the I_1, I_2 and I_3 curve fits is then propagated in to the calculated gain and spontaneous spectrums and this error is amplified in the SLD EL calculated spectrum. The results can be seen in Figure 3-12.

An equation consisting of the addition of two Gaussian curves was used to curve fit the improved segmented contact intensity data I_1, I_2, and I_3. The two Gaussians were used to pronounce SLD EL spectrum excited state peak emission and the ground state peak emission, causing a dip between the two. This is more consistent with the measured spectra. Each Gaussian curve peak was tuned to the ground state and excited state emission of I_1, I_2, and I_3. The curve fitted intensity spectrums were then plugged in to the

gain equation, Eqn 2-14, and the spontaneous emission, Eqn 2-16, and the resulting spectrums were plugged in to Eqn 2-9. The improved segmented contact intensity spectrums for 8ma and 180ma were curve fitted in this way and the coefficients can be seen in Table 3-3. The resulting SLD EL spectrum is not in good agreement with the actual data or the SLD EL spectrum calculated from the actual data I_1, I_2, and I_3. Again, the error produced during curve fitting is responsible for the bad agreement. The results can be seen in Figure 3-13.

In an effort to create fitted SLD EL spectrums which are in good agreement with the SLD EL spectrums calculated from the actual data, the gain and spontaneous emission spectrums were calculated from the original data, and then curve fitted with polynomials. This reduces the amount of error produced in the fitted curves. Again this was done for improved segmented contact intensity spectrums at 180ma and 8ma and the coefficients can be seen in Table 3-4. The results are in better agreement with the actual SLD spectrum and the SLD spectrums calculated from the original improved segmented contact method data, than the previous two curve fitting attempts. The results can be seen in Figure 3-14.

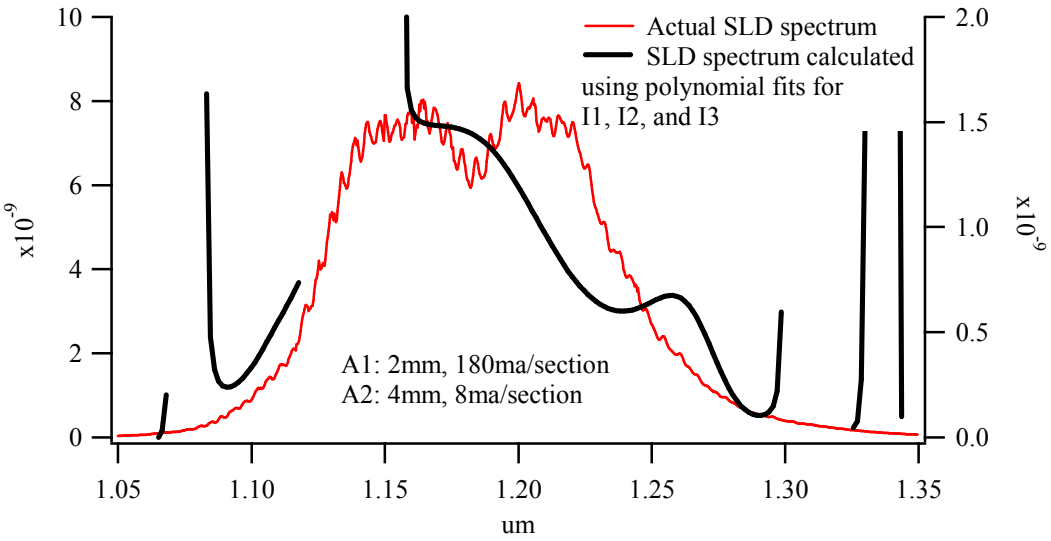

(a)

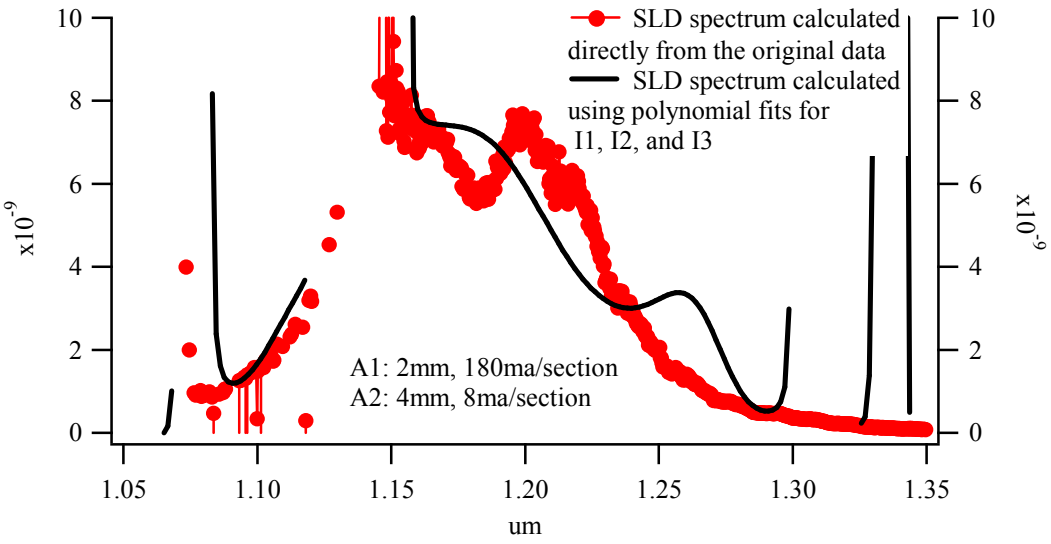

(b)

Figure 3-12. SLD EL spectrum calculated from polynomial fits of I_1, I_2, and I_3 compared to (a) the actual SLD EL spectrum and (b) the SLD EL spectrum calculated from the actual data I_1, I_2, and I_3

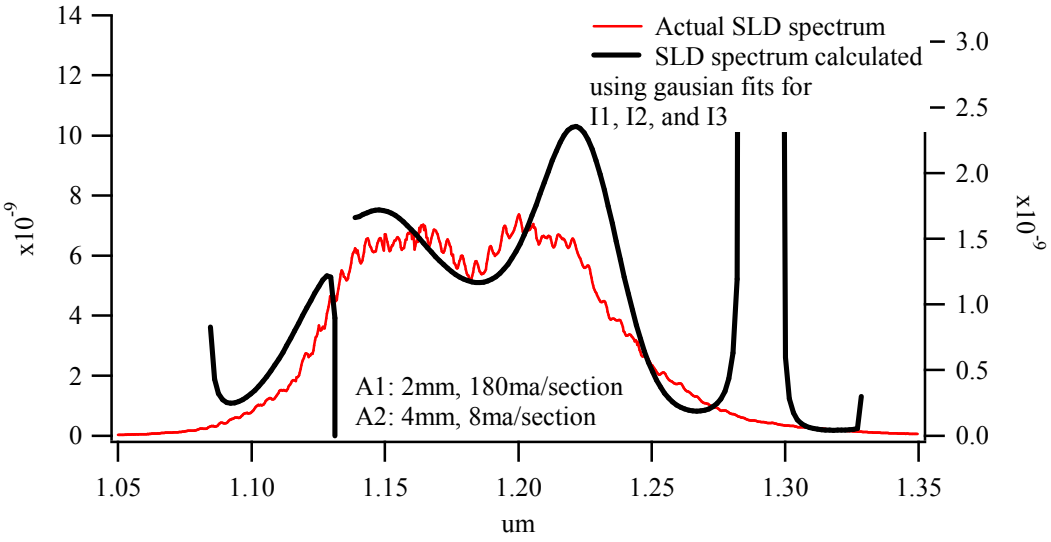

(a)

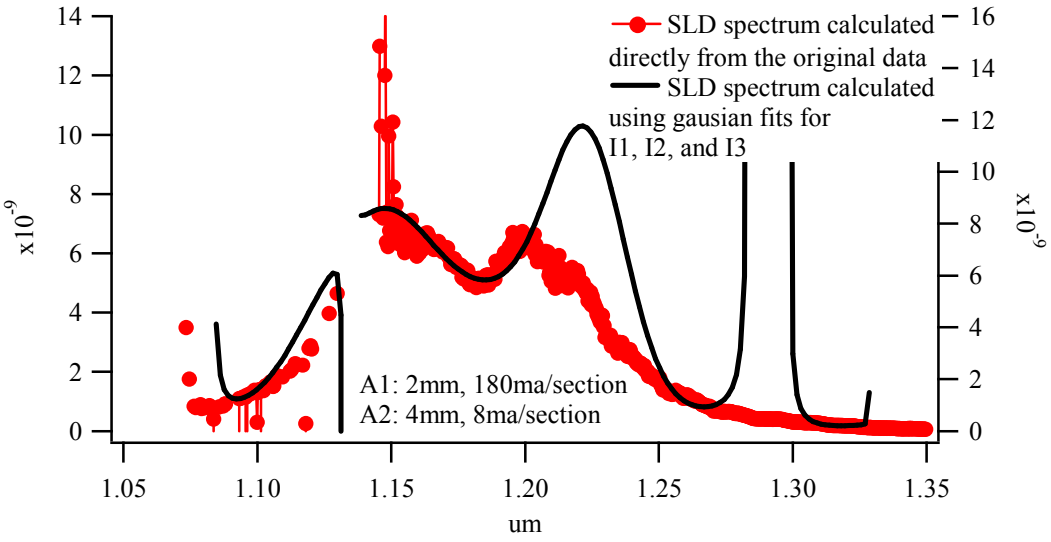

(b)

Figure 3-13. SLD EL spectrum calculated from Gaussian fits of I_1, I_2, and I_3 compared to (a) the actual SLD EL spectrum and (b) the SLD EL spectrum calculated from the actual data I_1, I_2, and I_3

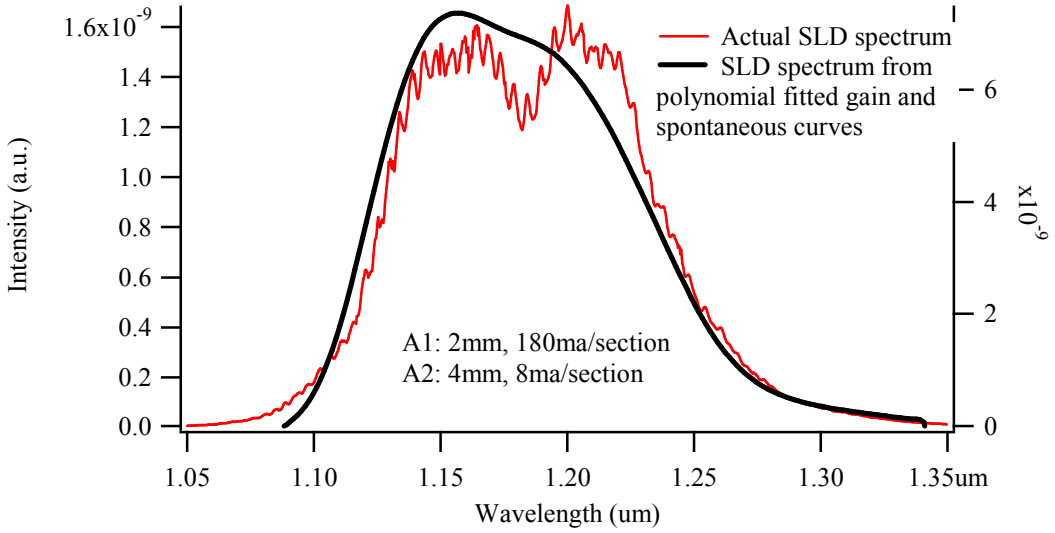

(a)

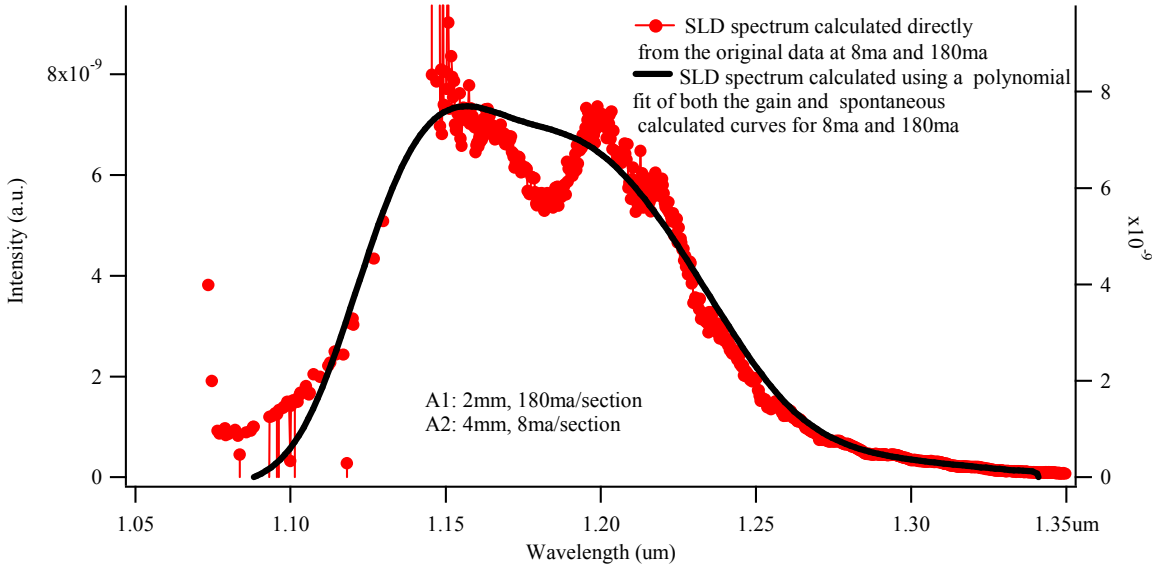

(b)

Figure 3-14. SLD EL spectrum calculated from polynomial fits of the gain and the spontaneous emission spectrums (a) the actual SLD EL spectrum and (b) the SLD EL spectrum calculated from the actual data I_1, I_2, and I_3

Polynomial Fits for 180mA I_1, I_2, and I_3				
Equation used:	$K_0+K_1x+K_2x^2\ldots$			
	Coefficients	180ma I_1 values	180ma I_2 values	180ma I_3 values
	K0	6.23E-06	-0.000915203	-0.0155541
	K1	-2.60E-05	0.00429876	0.0600921
	K2	4.33E-05	-0.00740069	-0.0720858
	K3	-3.58E-05	0.00453893	0.00700383
	K4	1.47E-05	0.00158713	0.0318364
	K5	-2.41E-06	-0.00277709	0.00407666
	K6		-0.000382711	-0.0143682
	K7		0.00185202	-0.00892168
	K8		-0.00096517	0.00306146
	K9		0.000164025	0.00665816
	K10			0.00173217
	K11			-0.00327504
	K12			-0.00218002
	K13			0.0024863
	K14			-0.000562205
Polynomial Fits for 8mA I_1, I_2, and I_3				
Equation used:	$K_0+K_1x+K_2x^2\ldots$			
	Coefficients	8ma I_1 values	8ma I_2 values	8ma I_3 values
	K0	9.52E-05	0.000262516	0.00050689
	K1	-0.000361591	-0.000990342	-0.00190731
	K2	0.000429095	0.00116414	0.00223449
	K3	-4.19E-05	-0.0001056	-0.000197237
	K4	-0.000196219	-0.000530213	-0.00101625
	K5	-1.26E-05	-3.86E-05	-7.71E-05
	K6	0.000100611	0.000269127	0.000514011
	K7	4.09E-05	0.000111725	0.000214943
	K8	-4.71E-05	-0.000124638	-0.000237207
	K9	-3.60E-05	-9.70E-05	-0.000185561
	K10	3.84E-05	0.000101852	0.000193958
	K11	-8.73E-06	-2.30E-05	-4.37E-05

Table 3-2. Polynomial fit coefficients for I_1, I_2, and I_3 at 180mA and 8mA

Gaussian Fits for 180mA I_1, I_2, and I_3				
Equation used:	y0+A0*exp(-(wave-1.2)^2/w0^2)+A1*exp(-(wave-1.14)^2/w1^2)			
	Coefficients	180ma I_1 values	180ma I_2 values	180ma I_3 values
	y0	-7.86E-11	6.23E-11	1.52E-10
	A0	3.25E-10	7.40E-10	1.71E-09
	A1	2.67E-10	9.45E-10	2.66E-09
	w0	0.136301	0.0761161	0.0522241
	w1	0.0889164	0.0528127	0.0373727
Gaussian Fits for 8mA I_1, I_2, and I_3				
Equation used:	y0+A0*exp(-(wave-1.24)^2/w0^2)+A1*exp(-(wave-1.175)^2/w1^2)			
	Coefficients	8ma I_1 values	8ma I_2 values	8ma I_3 values
	y0	7.57E-12	7.91E-12	5.99E-12
	A0	1.93E-10	3.30E-10	4.76E-10
	A1	1.28E-10	1.51E-10	1.65E-10
	w0	0.0426573	0.0437862	0.0434402
	w1	0.0411964	0.0379459	0.0366956

Table 3-3. Gaussian fit coefficients for I_1, I_2, and I_3 at 180mA and 8mA

Polynomial Fits for 180mA Gain and Spontaneous Spectra			
Equation used:	$K_0+K_1x+K_2x^2\ldots$		
	Coefficients	180ma G values	180ma S values
	K0	-1.68E+07	-0.00159392
	K1	8.25E+07	0.00502039
	K2	-1.68E+08	-0.00439033
	K3	1.84E+08	-0.00090012
	K4	-1.12E+08	0.00208136
	K5	3.67E+07	0.000875023
	K6	-5.00E+06	-0.000991724
	K7		-0.000711185
	K8		0.000797269
	K9		-0.000186992
Polynomial Fits for 8mA Gain and Spontaneous Spectra			
Equation used:	$K_0+K_1x+K_2x^2\ldots$		
	Coefficients	8ma G values	8ma S values
	K0	-1.98E+07	-0.00745238
	K1	7.98E+07	0.0262674
	K2	-1.28E+08	-0.029559
	K3	1.03E+08	0.00315994
	K4	-4.16E+07	0.014207
	K5	6.69E+06	-0.00282305
	K6		-0.00840134
	K7		0.00571228
	K8		-0.00111187

Table 3-4. Polynomial fit coefficients for gain and spontaneous spectra at 180mA and 8mA

3.7 Summary

In this chapter a method for measuring SLD EL spectrums with many different possible configurations was discussed. Each step was discussed more thoroughly and included technical testing details. The simulation results confirm that with a longer cavity length the maximum bandwidth narrows. A graph comparing power and bandwidth can be used to help find the optimum configuration of power and bandwidth. A comparison of the measured SLD EL spectrum with the simulated SLD EL spectrum shows that they are in good agreement, and confirms that the SLD equation is effective in predicting the SLD EL spectrum for p-doped quantum dot material. The data obtained from the improved segmented contact method was curve fitted. The predicted SLD EL spectrums with the best agreement to the actual SLD EL spectrum were calculated from polynomial fitted gain and spontaneous spectrums.

Chapter 4 - Summary and Future Work

4.1 Summary

This thesis was dedicated to the quantum dot multi-section SLD. A SLD is typically an edge emitting device which has higher power than a typical LED and a broader bandwidth compared to a laser. The SLD output is amplified spontaneous emission. Superluminescent diodes are used in a variety of applications, however the multi-section SLD in this project is intended for OCT. OCT requires broad bandwidth and high power. The optimum center wavelength is different for each application. For use on skin a wavelength of 1.2um is desirable. One goal of this experiment was to achieve a SLD device with a wide bandwidth and a reasonable power. While the SLD is not the only option for OCT, it is cheaper and simpler to use. There are several different methods that are being used to create SLDs for OCT, however the multi-section SLD is unique in that it allows for the tuning of both the ground state and the excited state to achieve a wide bandwidth and a high power. This is important because it allows more power and bandwidth to be extracted from a given quantum dot material than most other methods, and the output can easily be coupled in to a fiber.

The multi-section SLD used in this project is composed of three regions, two gain sections and one absorber section. The front gain section is pumped at a high current density to achieve excited state emission. The second gain section is pumped with a lower current density to achieve ground state emission. For optimum power, the front section is biased at the current density where power saturates. The multi-section SLD EL spectrum can be simulated with an equation developed by Y. C. Xin. One purpose of this

project was to verify that this equation works for non-traditional quantum dot SLD devices. The equation requires gain, spontaneous emission, and lengths for each gain section. With a multi-section SLD there are a number of possible configurations. The SLD equation can simulate several configurations, and predict several optimum bandwidths with different cavity lengths and gain section length ratios. This process saves time and reduces the amount of wear on the device from un-necessary testing.

The gain is found using the improved segmented contact method, which is based off of the segmented contact method. Unless there is a cumbersome slit placed in front of the emitting facet, the segmented contact method ignores the error produced by unguided spontaneous emission, and while this method works for quantum well devices, it is not sufficient for quantum dot devices. Quantum dots active media have a much smaller optical gain and unguided spontaneous emission cannot be ignored. The improved segmented contact method uses EL spectrums from three different lengths to subtract out the unguided spontaneous emission, resulting in a cleaner gain spectrum. The pure spontaneous emission spectrum can be calculated from the same measured data used to calculate the gain.

A SLD which has a peak wavelength of 1200nm, a power greater than 0.2mW, a bandwidth greater than 100nm, and a dip between the ground and excited state emission of less than 3dB was achieved. This SLD device will work for OCT. It was also verified that the SLD equation simulations were in good agreement with the actual data, showing that the equation used to describe the electroluminescence (EL) spectrum of the multi-section SLD works when applied to different quantum dot material.

4.2 Future Work

The multi-section concept is being incorporated into a more complex SLD design, similar to the V-groove etched tapered waveguide device mentioned in Chapter 1. This novel multi-contact device is being developed by Professor Hogg's group at The University of Sheffield. They are achieving 2mW of power under CW conditions with a bandwidth of about 75nm. The device emits at a peak wavelength of 1050nm, which is associated with zero dispersion in aqueous tissue such as the eye [1]. The front output facet is angled with respect to the facet normal. The ridge is 7um wide and is divided in to 1mm electrically isolated sections. The total device length is 10mm. The 1mm long back section tapers into a 300um wide ridge, which is left un-pumped to act as an absorber. The rear facet is a tilted deep v-groove etch facet. The active region consists of chirped quantum dots.

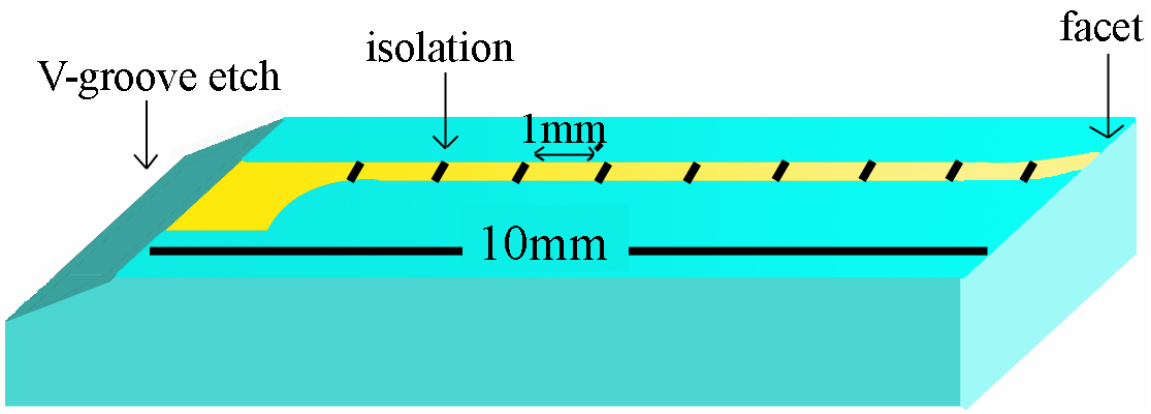

Figure 4-1. Multi-contact SLD with V-groove etch and tapered waveguide. Each isolated section is 1mm long. The total device length is 10mm.

4.3 References

[1] A. F. Fercher, W. Drexler, C. K. Hitzenberger and T. Lasser: “Optical coherence tomography— principles and applications” Rep. Prog. Phys., vol. 66, pp 239-303, 2003